New polycyclic dual inhibitors of the wild type and the V27A mutant M2 channel of the influenza A virus with unexpected binding mode

Postprint version of the published paper https://doi.org/10.1016/j.ejmech.2015.04.030

Matias Rey-Carrizo[a], Sabrina Gazzarrini[b], Marta Frigolé-Vivas[a], Salomé Llabrés[c], Jordi Juárez-Jiménez[c], Mercè Font-Bardia[d], Lieve Naesens[e], Anna Moroni[b], Francisco J. Luque[c], and Santiago Vázquez[a,*]

[a]*Laboratori de Química Farmacèutica (Unitat Associada al CSIC), Facultat de Farmàcia, and Institute of Biomedicine (IBUB), Universitat de Barcelona, Av. Joan XXIII, s/n, Barcelona, E-08028, Spain*

[b]*Department of Biosciences and National Research Council (CNR) Biophysics Insititute (IBF), University of Milan, Via Celoria 26, 20133 Milan, Italy*

[c]*Departament de Fisicoquímica, Facultat de Farmàcia, and Institute of Biomedicine (IBUB), Universitat de Barcelona, Av. Prat de la Riba 171, Santa Coloma de Gramenet E-08921, Spain*

[d]*Unitat de Difracció de RX, Centres Científics i Tecnològics (CCiTUB), Universitat de Barcelona, Solé i Sabarís 1-3, Barcelona, E-08028, Spain*

[e]*Rega Institute for Medical Research, KU Leuven, B-3000 Leuven, Belgium*

[*]Corresponding author. Tel.: +34-934-024-533; e-mail: svazquez@ub.edu

Abstract:

Two new polycyclic scaffolds were synthesized and evaluated as anti-influenza A compounds. The 5-azapentacyclo[6.4.0.0^{2,10}.0^{3,7}.0^{9,11}]dodecane derivatives were only active against the wild-type M2 channel in the low-micromolar range. However, some of the 14-azaheptacyclo[8.6.1.0^{2,5}.0^{3,11}.0^{4,9}.0^{6,17}.0^{12,16}]heptadecane derivatives were dual inhibitors of the wild-type and the V27A mutant M2 channels. The antiviral activity of these molecules was confirmed by cell culture assays. Their binding mode was analysed through molecular dynamics simulations, which showed the existence of distinct binding modes in the wild type M2 channel and its V27A variant.

Keywords:

Amantadine, polycyclic amines, influenza A, M2 channel, V27A mutant, molecular dynamics.

Highlights

a) Several polycyclic amines are synthesized as anti-influenza A virus.
b) One of the syntheses presents a one-pot decarbonylation/intramolecular Diels-Alder reaction.
c) Compounds were examined as M2 channel blockers and anti-influenza A agents through *in vitro* tests.
d) All the compounds were active against the wild-type M2 channel and two against the V27A mutant.
e) Molecular simulations suggest distinct binding modes for the wild-type and V27A channels.

1. Introduction

Influenza viruses cause the seasonal flu, which is worldwide associated with high socio-economic and medical burden [1]. Besides, influenza A virus possesses the capacity to cause sudden pandemics having higher mortality rates [2], such as the dreadful Spanish flu in 1918 [3,4] or the H1N1 pandemic in 2009 caused by a swine-origin influenza virus [5–8]. There is also increased vigilance that highly pathogenic avian influenza viruses such as H5N1 [9] or H7N9 [10] may potentially acquire human-to-human transmission, which may have devastating consequences. Though highly recommended for primary prophylaxis, the current influenza vaccines present several drawbacks [11], and hence antiviral drugs are equally vital for prevention and treatment of influenza infections. Only four anti-influenza drugs are available at this time: two neuraminidase inhibitors (oseltamivir and zanamivir) and two M2 channel blockers (amantadine, Amt, and rimantadine) [12]. Most of the circulating strains are Amt-resistant [13,14], which has compelled the Centers for Disease Control and Prevention to deter its use [15]. On the other hand, oseltamivir resistance has also been spreading [16,17] and dual resistance to both oseltamivir and Amt has been detected [18]. These reasons have prompted the quest for new antivirals as effective ways of fighting influenza.

The influenza A M2 polypeptide (A/M2) of 97 amino acids long, forms a homotetrameric proton channel that is critical for virus replication [19]. In the viral life cycle, A/M2 is crucial for acidification of the interior of the virus which is required for uncoating of the viral genetic material inside the host cell [20]. Furthermore, A/M2 regulates the intralumenal pH of the Golgi apparatus and in this way prevents the premature conformational change of hemagglutinin, another key viral protein [21]. The A/M2 protein is also the target of Amt and hence Amt-resistant influenza strains bear a mutated Amt-insensitive M2 channel. Although many mutations appear to be viable *in vitro* [22,23], only three mutants comprehend more than 99% of the reported resistance [24,25], namely L26F, V27A and S31N. Despite the fact that the S31N amino acid substitution is predominant in more than 98% of the mutated M2 channels found in H3N2 viruses [26], the V27A mutant has been isolated in 10-77% of influenza viruses, depending on the viral strain and season [24,27]. Furthermore, the V27A mutant has proved to be the only one among the three most prevalent mutations to be originated from drug selection pressure [25]. Finally, while the S31N and L26F mutants are

sensitive, to some extent, to Amt, the latter is completely ineffective against the V27A mutant M2 channel. Therefore, there is great interest in the development of molecules capable of blocking multiple M2 channels to prevent the virus from finding an escape mechanism.

Wu et al. have very recently reported the synthesis of *N*-[(5-bromothiophen-2-yl)methyl]adamantan-1-amine, **1**, the first dual inhibitor of wild-type (wt) and S31N mutant M2 channels [28]. Our work has been focused on the V27A mutant M2 channel, describing pyrrolidine **2**, the most potent dual inhibitor of wt (IC_{50} = 3.4 μM) and V27A (IC_{50} = 0.29 μM) mutant M2 channels [29] (Figure 1). Last year, we reported the triple inhibitor **3**, which is active against wt (IC_{50} = 18.0 μM), V27A (IC_{50} = 0.70 μM) and L26F (IC_{50} = 8.6 μM) mutant M2 channels [30]. Good activities against both wt (IC_{50} = 2.1 μM) and V27A (IC_{50} = 22.6 μM) mutant M2 channels were found with polycyclic guanidine **4** [30] (Figure 1), which inspired us to derivatize it in pursue of potent inhibitors of the V27A A/M2 mutant protein.

Herein we describe the syntheses and pharmacological evaluations of two families of polycyclic amines. One of them was designed with an enlarged scaffold with respect to **4** in order to explore the chemical space around this skeleton, and the other features a new small polycyclic structure that was also assessed. All the novel compounds were low micromolar inhibitors of the wt M2 channel, and one of them was found to be a submicromolar inhibitor. Besides, amine **10** and guanidine **12** were active blockers of the V27A mutant M2 channel, but strikingly the amine derivative was more potent than the guanidine.

Figure 1.

2. Results and discussion

2.1. Chemistry

Our interest in modifying the polycyclic scaffold of Amt for developing novel M2 channel blockers has led to the syntheses of ring-contracted, ring-rearranged and 2,2-dialkyl derivatives of amantadine [31–34]. While exploring new carbon skeletons, we unveiled compound **4** as the only dual inhibitor of its family, with a low micromolar

IC_{50} against wt M2 channel (IC_{50} = 2.1 μM), and a mid-range IC_{50} against the V27A mutant (IC_{50} = 22.6 μM) [30] (Figure 1). From previous molecular dynamics studies [30], we assumed that both wt and V27A M2 channels may accommodate larger molecules than **4**. Since compound **4** was available in a few synthetic steps, we aimed at enlarging the molecule to evaluate its effects on the blockade of the M2 channels. On the other hand, we were also keen on the development of another small family of compounds easily available in a short synthetic sequence.

The synthesis of the first set of compounds, derivatives of **4**, started with known imide **5** easily accessed through the reaction of maleimide and cycloheptatriene [35]. The Diels-Alder reaction of **5** with 5,5-dimethoxy-1,2,3,4-tetrachlorocyclopentadiene furnished adduct **6** in 89% yield. This one was subjected to a one-pot dechlorination/deprotection reaction. The dechlorination was carried out by metallic sodium in liquid ammonia and an acidic deprotection of the acetal finally produced keto-imide **7** in 41% overall yield. Submitting **7** to 180 ºC in a sealed tube in the presence of hydroquinone as an antioxidant, produced polycyclic imide **8** through a one-pot decarbonylation coupled with an intra-molecular Diels-Alder reaction [36], in 44% yield over the two steps (Scheme 1). Of note, the reaction started with the retrocheletropic extrusion of a molecule of carbon monoxide followed by two disrotatory retroelectrocyclic rearrangements that provided a molecule with the suitable configuration for the intramolecular Diels-Alder reaction (Scheme 2). Imide **8** was further reduced to amine **9**, and was subsequently submitted to a catalytic hydrogenation to yield saturated amine **10**. Both amines were transformed into their corresponding guanidines **12** and **11** respectively, after being reacted with 1*H*-pyrazole-1-carboxamidine in moderate yields (Scheme 1).

Scheme 1.

Scheme 2.

In order to explore other polycyclic scaffolds to assess their potential as M2 channel blockers, we also synthesized a second small set of compounds. Taking known diester **13** as the first building block [37], a basic hydrolysis was performed upon this molecule to obtain diacid **14** in 86% yield. Unfortunately, we could not reproduce the photochemical reaction of **14** described in the literature to afford polycyclic structure **15**

[37], even though the reaction was also attempted with the diester **13** and the anhydride of diacid **14**. The synthesis was pursued with the hydrogenation of **14** at high pressure of hydrogen to furnish saturated diacid **16** [38] as the single *endo*-stereoisomer, which was confirmed with the X-ray diffraction analysis of a subsequent derivative. In turn, **16** was reacted with urea at high temperature in order to secure imide **17** in 79% yield, which was further reduced to amine **18**. The stereoisomerism of this family of compounds was unequivocally determined with the X-ray crystal structure of **18**, which disclosed the *endo*-stereoisomer (Figure 2) [39]. Finally, amine **18** was transformed into the guanidine derivative **19** by reaction with 1*H*-pyrazole-1-carboxamidine (Scheme 3).

Figure 2.

Scheme 3.

2.2. Inhibition of wt A/M2 and amantadine-resistant mutant ion channels

The inhibitory activity of the compounds was tested on A/M2 channels expressed in *Xenopu*s oocytes, using the two-electrode voltage clamp (TEVC) technique. All inhibitors were initially tested at 100 µM. Then, the compounds that inhibited either wt or V27A M2 channel activity by more than 70% were chosen for measurement of their IC_{50} value in an isochronic (2 min) inhibition assay. The results are given in Table 1.

Table 1

Amt inhibited the wt A/M2 channel with an IC_{50} of 16.0 µM, displayed less activity against the S31N mutant with an IC_{50} of 200 µM, and was totally inactive against the V27A variant. Amines **9** and **10** as well as guanidines **11** and **12** exhibited a low micromolar activity against the wt channel, but surprisingly, both amines were more active than their guanidine derivatives, a behaviour opposed to the results reported for previous sets of molecules [29,30]. The terminal insaturation seemed to have little to no effect on the activity against the wt M2 channel (**9** vs. **10** or **11** vs. **12**). However, against the V27A mutant, only the saturated compounds **10** and **11** displayed inhibitory activity, both being micromolar blockers of this M2 channel variant. Again, amine **10** was more active than guanidine **11** (Table 1). Intriguingly, amine **10** was more active against the V27A mutant than its precursor guanidine **4** (Figure 1) while retaining the same activity against the wt channel. This confirmed our initial hypothesis about the potential optimization of this scaffold against the V27A mutant M2 channel.

Besides, compounds **18** and **19** were both, at least, low micromolar inhibitors of the wt channel, since guanidine **19**, presenting a submicromolar activity, was more potent than its parent amine **18**. Unfortunately, none of them were active against the V27A mutant. Neither of the tested molecules showed any relevant activity against the S31N mutant M2 channel.

2.3. Molecular modeling

The pharmacological profile of the size-expanded compounds **9** and **10**, specifically as inhibitors of the V27A mutated channel, prompted us to explore their binding mode to the wt M2 channel and its V27A variant. To this end, a series of MD simulations were performed for the ligands bound to the M2 channels following the computational strategy reported previously for the binding of the Amt to both wt and V27A M2 channels [30]. In particular, MD simulations were started from equilibrated structures of the channel embedded in a lipidic bilayer, and the ligand was located in the channel pore in the *down* orientation, which denotes that the protonated amine group is pointing toward the His plane (for details see Experimental details and ref. 30).

The analysis of the MD simulations run for the wt M2 channel revealed a consistent binding mode for **9** and **10**. Thus, the centre-of-mass (COM) of the ligand was located close to the plane formed by the S31 Cα atoms, with the amine nitrogen pointing to the H37 plane (average distance of 6.2 and 5.8 Å for **9** and **10**, respectively; see Figures S1 and S3 in Supplementary Material). Moreover, the tilt angle of the compounds, chosen as a measure of the deviation of the amine nitrogen from the pore axis, was 13.9 and 17.6 degrees for **9** and **10**, respectively (Figure 3). Overall, these trends resemble the binding mode reported for Amt in previous MD simulations [30] as well as in the crystallographic structure 2KQT [40], in agreement with the similar inhibitory activity of these inhibitors (Table 1).

In contrast to these findings, the MD simulations run for the V27A channel suggest that compounds **9** and **10** adopt a distinct orientation, likely due to the wider pore of the channel [30]. Thus, in five out of six replicas run for **9** and **10** the inhibitor was found in the *up* binding mode, with the amine nitrogen oriented opposite to the plane formed by the H37 tetrad (Figure 3). The COM of the compounds was located between the planes formed by the Cα atoms of the S31 and A27 tetrads, the nitrogen amine was on average

located 15.3 and 15.0 Å from the H37 Cα plane for **9** and **10**, respectively, and the tilt angle was close to 152 degrees for the two compounds (see Figures S2 and S4 in Supplementary Material).

Figure 3.

Previous molecular modeling studies showed that Amt also adopted the *up* binding mode in the V27A channel [30] and eventually was released from the channel pore, in agreement with the weak inhibition of the mutated channel (10.8% inhibition at 100 μM; Table 1). In contrast to Amt, the MD simulations run for compounds **9** and **10** support the stability of the *up* binding mode along the whole trajectory. This trend was also found for the binding of the pyrrolidine derivative 7,8,9,10-tetramethyl-3-azapentacyclo[7.2.1.$1^{5,8}$.$0^{1,5}$.$0^{7,10}$]-tridecane **3** (Scheme 3; note that **3** corresponds to compound **18** in ref. 30). This agrees with the higher inhibitory potency of these compounds, as noted in IC_{50} values of 17.2 and 0.70 μM for **10** and **3**, respectively. Noteworthy, the involvement of flipped orientations upon inhibitor binding to the wt M2 channel and its S31N variant has also been recently reported [28].

Compared to Amt, even though the size-enlargement of the hydrophobic cage has little effect on the inhibitory potency against the wt channel (IC_{50} values of 16.0, 2.6, 2.1 and 18.0 μM for Amt, **9**, **10** and **3**, respectively), it affords a differential stabilization against the V27A channel. This trend can be attributed to the larger size of these compounds, as noted in molecular surfaces of 202, 255 and 260 $Å^2$ for Amt, **9** and **10**, respectively (molecular volumes of 220, 293 and 304 $Å^3$ for Amt, **9** and **10**), leading to a more stabilizing van der Waals interaction with the V27A channel (average values of -21.3, -32.3 and-34.8 kcal/mol for Amt, **9** and **10**, respectively, as determined from the snapshots sampled in the three replicas run for each inhibitor). On the other hand, the larger inhibitory potency of **10** could also reflect the increase in hydrophobicity resulting from saturation of the double bond present in **9**, as noted in the logP values of 4.8 and 4.3 estimated for **10** and **9** from IEF-MST computations. Note that this trend is also found in the guanidine derivatives **11** and **12**, where the saturated compound also exhibits a larger hydrophobicity (estimated logP values of 3.2 and 2.5 for **11** and **12**, respectively).

2.4. Antiviral activity and cytotoxicity in cell culture

The anti-influenza virus activity of the compounds was first assessed in a relatively stringent three-day cytopathic effect (CPE) reduction assay in MDCK cells (Table 2). None of the tested compounds displayed any activity against the A/PR/8/34 strain bearing a doubly mutated M2 channel (V27T and S31N), in agreement with the TEVC results, nor against the A/HK/7/87 strain which carries a wt M2 channel. A plausible reason for the inactivity of compounds **9**, **10**, **11** and **12** against the A/HK/7/87 strain could be their poor selectivity, since all four compounds exhibited high cytotoxicity after 72 hr incubation with the cells. This was not the case for **18** and **19** (Table 2). None of the tested compounds was active against the influenza B virus B/HK/5/72 (data not shown).

Table 2.

We subsequently performed a 24-hr virus yield assay (based on RT-qPCR quantification of virus in the supernatant) and a virus plaque reduction assay (PRA), both using the wt M2 A/HK/7/87 virus. In the PRA, both amines **9** and **10** were found to be active in the same order of magnitude as Amt, but neither of the guanidines **11** nor **12** showed any activity (Figure 4). With regard to the second family of compounds, only **18** was found to have intermediate antiviral activity, since guanidine **19** was completely inactive. For amine **10**, the antiviral activity was close to its cytotoxic concentration (CC_{50}; Table 2), meaning that it has a narrow selectivity index. The antiviral data in the PRA were confirmed with the virus yield assay, where amine **10** was shown to be inactive as well as guanidines **11** and **12**. On the other hand, amines **9** and **18** exhibited visible antiviral activity giving 2-$\log_{10}$ reduction in virus yield. These combined *in vitro* data showed that **9** was the more potent compound, although associated with some cytotoxicity. The activity of **18** against the wt M2 channel, as seen in the TEVC studies, was supported by the cell culture assays with no visible cytotoxicity at the concentrations tested.

Figure 4.

3. Conclusions

Two novel series of size-expanded polycyclic amines and guanidines have been synthesized and tested as potential inhibitors of influenza A virus. The novel compounds were all low micromolar inhibitors of the wt M2 channel, and one of the guanidine derivatives (**19**) was found to be a submicromolar inhibitor with an IC_{50} value of 0.84 μM. On the other hand, amine **10** and guanidine **11** were active blockers of the V27A mutant M2 channel, but strikingly the amine derivative was more potent than the guanidine. Molecular modeling studies suggest a distinct binding mode for these Amt-related analogues to the wt M2 channel and its V27A variant. Compared to Amt, the stronger inhibitory potency of these compounds seems to arise from the enhanced size of the hydrophobic cage of amine **10**. The inhibitory activity of this compound was confirmed in the virus plaque reduction assay.

4. Experimental section

4.1. Plasmid, mRNA synthesis and microinjection of oocytes

The cDNA encoding the influenza A/Udorn/72 (A/M2) was inserted into pSUPER vector for the expression on *Xenopus* oocyte plasma membrane. A/M2 S31N and A/M2 V27A mutants were generated by QuikChange site-directed mutagenesis kit (Agilent Technologies). The synthesis of mRNA and microinjection of oocytes have been described previously [42].

4.2. Two-electrode voltage clamp analysis

Macroscopic membrane current was recorded 24-72 hours after injection as described previously [43]. Oocytes were perfused at room temperature in Barth's solution containing (in mM) 88 NaCl, 1 KCl, 2.4 $NaHCO_3$, 0.3 $NaNO_3$, 0.71 $CaCl_2$, 0.82 $MgCl_2$, and 15 HEPES for pH 8.5 or 15 MES for pH 5.5 at a rate of 2 mL/min. The tested compounds were dissolved in DMSO and applied (100 μM) at pH 5.5 when the inward current reaches maximum. The compounds were applied for 2 min, and residual membrane current was compared with the membrane current before the application of compounds. Currents were recorded at −20 mV and analyzed with pCLAMP 8 software package (Axon Instruments, Sunnyvale, CA).

4.3. Antiviral evaluation in cell culture

To determine the anti-influenza virus activity in Madin-Darby canine kidney (MDCK) cells, CPE reduction and virus yield assays were performed as described [41, 44]. Briefly, MDCK cells grown in 96-well plates were infected with influenza virus [strains A/PR/8/34 (A/H1N1); A/HK/7/87 (A/H3N2) or B/HK/5/72], and at the same time the tested compounds were added in serial dilutions. After 72 h incubation at 35 ºC, microscopy was performed to score the compounds' inhibitory effect on viral cytopathic effect (CPE) as well as their cytotoxicity. These data were verified by measuring the cell viability with the formazan-based MTS assay. In separate experiments, supernatants were harvested from the infected and compound-treated cells at 24 h post infection, and virus yield in these samples was determined by RT-qPCR. To perform plaque reduction assays, influenza virus A/HK/7/87 was added together with different concentrations of the compounds, to confluent MDCK cells in 12-well plates. After 1 h incubation at 35°C, excess virus was removed and replaced by fresh medium containing the compounds and 0.8% agarose. After 72 h incubation, plaques were visualized by cell fixation with 3.7% formaldehyde and staining with 0.1% crystal violet.

4.4. Cytotoxicity assays

The compound cytotoxicity was assessed as described [44]. Briefly, exponentially growing MDCK cells were grown in 96-well plates and the test compounds were added in serial dilutions. After 72 h incubation at 35 °C, cell viability was measured by the formazan-based MTS assay and the OD values were used to calculate the compound concentrations causing 50% cytotoxicity (CC_{50}).

4.5. Chemistry

4.5.1. General

Melting points were determined in open capillary tubes. NMR spectra were recorded in the following spectrometers: ^{1}H NMR (400 MHz), ^{13}C NMR (100.6 MHz). Chemical shits (δ) are reported in ppm related to internal tetramethylsilane (TMS) and coupling constants are reported in Hertz (Hz). Assignments given for the NMR spectra are based on DEPT, COSY $^{1}H/^{1}H$, HETCOR $^{1}H/^{13}C$ (HSQC and HMBC sequences for one bond and long range $^{1}H/^{13}C$ heterocorrelations, respectively) and NOESY experiments for

selected compounds. For the MS and GC/MS analyses the sample was introduced directly or through a gas chromatograph. For GC/MS analyses a 30–meter column [5% diphenyl–95% dimethylpolysiloxane, conditions: 10 psi, initial temperature: 35 ºC (2 min), then heating at a range of 8 ºC/min till 300 ºC, then isothermic at 300 ºC] was used. The electron impact (70 eV) or chemical ionization (CH_4) techniques were used. Only significant ions are given: those with higher relative ratio, except for the ions with higher *m*/*z* values. Accurate mass measurements were obtained using ESI technic. Absorption values in the IR spectra (KBr or ATR) are given as wave-numbers (cm^{-1}). Only the more intense bands are given. Column chromatography was performed on silica gel, 60 Å (35-70 mesh, SDS). For the thin layer chromatography (TLC) aluminum-backed sheets with silica gel 60 Å F254 were used and spots were visualized with UV light and/or 1% aqueous solution of $KMnO_4$.

*4.5.2. (1R, 2S, 3R, 4R, 7S, 8S, 9R, 10S, 11S, 15R)-4,5,6,7-Tetrachloro-18,18-dimethoxy-13-azahexacyclo[8.5.2.1^{4,7}.0^{2,9}.0^{3,8}.0^{11,15}]octadeca-5,16-diene-12,14-dione (**6**)*

A mixture of **5** [35] (4.00 g, 19.88 mmol) and 5,5-dimethoxy-1,2,3,4-tetrachlorocyclopentadiene (11.30 mL, 64.41mmol) were mixed in a sealed tube and heated to 140 ºC overnight. The brownish paste was concentrated under vacuo and the crude was purified by silica column chromatography. The EtOAc fractions carried **6** as a light yellow solid (8.23 g, 89%), mp> 300 ºC. IR ν 3366, 3048, 2987, 2948, 1761, 1717, 1451, 1338, 1296, 1231, 1176, 1119, 1031, 981, 938, 830, 794, 777, 750, 702, 661, 631, 611 cm^{-1}. ^{1}H NMR (400 MHz, $CDCl_3$) δ: 2.11 [m, 2 H, 2(9)-H], 2.54 [m, 2H, 3(8)-H], 2.74 [t, *J* = 1.2 Hz, 2 H, 11(15)-H], 3.26 [m, 2 H, 1(10)-H], 3.49 [s, 3H, -OC$\underline{H}_3$], 3.51 [s, 3H, -OC$\underline{H}_3$], 6.43 [dd, *J* = 4.4 Hz, *J'* = 3.2 Hz, 2 H, 16(17)-H], 7.95 (broad s, 1 H, NH). ^{13}C NMR (100.6 MHz, $CDCl_3$) δ: 34.8 [CH, C1(10)], 38.1 [CH, C2(9)], 43.7 [CH, C11(15)], 50.4 [CH, C3(8)], 51.8 [CH_3, -O$\underline{C}H_3$], 52.3 [CH_3, -O$\underline{C}H_3$], 76.7 [C, C4(7)], 128.8 (C, C18), 130.7 [C, C5(6)], 133.1 [CH, C16(17)], 177.7 [C=O, C12(14)]. MS (GC), rt = 31.1 min, m/e (%); main ions: 430 [(M-Cl) $^+$, 100], 295 (12), 281 (25), 255 (94), 207 (80), 179 (15), 112 (25), 103 (18), 78 (95), 59 (66). HRMS-ESI+ m/z [*M*+H]$^+$ calcd for [$C_{19}H_{17}Cl_4NO_4$+H]$^+$: 463.9984, found: 463.9978.

*4.5.3. (1R, 2S, 3R, 4R, 7S, 8S, 9R, 10S, 11S)-13-Azahexacyclo[8.5.2.1^{4,7}.0^{2,9}.0^{3,8}.0^{11,15}]octadeca-5,16-diene-12,14,18-trione (**7**).*

A solution of **6** (9.00 g, 19.3 mmol) in dry THF (60 mL) and dry MeOH (9 mL) was carefully added to freshly distilled ammonia (500 mL aprox.) at - 60 ºC. Sodium (5.6 g, 24.2 mmol) was carefully added in small portions over 15 min. The dark blue solution was stirred for another 15 min and it was quenched with NH_4Cl. The white suspension was allowed to warm up to room temperature and was stirred overnight. The white precipitate was acidified with HCl aq. 10% (200 mL) and was left stirring for 1 hour. The white solution was extracted with DCM (3 x 150 mL), the organic phase was dried over Na_2SO_4, filtered and concentrated under vacuo. The white solid obtained was purified by silica column chromatography. In the (DCM : MeOH, 0.8%) fractions **7** was recovered as a white solid (2.24 g, 41%), mp 202-203 ºC. IR ν 3263, 3083, 3040, 2997, 2939, 1795, 1780, 1695, 1363, 1297, 1226, 1193, 1104, 1067, 999, 941, 888, 879, 717, 686 cm^{-1}. ^{1}H NMR (400 MHz, $CDCl_3$) δ: 1.85 [m, 2 H, 2(9)-H], 2.33 [td, *J* = 3.2 Hz, *J'* = 2 Hz, 2 H, 3(8)-H], 2.64 [t, *J* = 1.6 Hz, 2 H, 11(15)-H], 2.99 [quin, *J* = 2.8 Hz, 2 H, 4(7)-H], 3.21 [m, 2 H, 1(10)-H], 6.46 [dd, *J* = 4.8 Hz, *J'* = 3.2 Hz, 2 H, 16(17)-H], 6.80 [t, *J* = 2 Hz, 5(6)-H], 8.03 (broad s, 1 H, NH). ^{13}C NMR (100.6 MHz, $CDCl_3$) δ: 35.2 [CH, C1(10)], 37.5 [CH, C3(8)], 41.7 [CH, C2(9)], 43.9 [CH, C11(15)], 50.1 [CH, C4(7)], 133.8 [CH, C16(17)], 134.0 [CH, C5(6)], 178.2 [C=O, C12(14)], 200.0 (C=O, C18). MS (GC), rt = 24.5 min, m/e (%); main ions: 253 [(M-CO)$^{\cdot+}$, 53], 187 (14), 175 (29), 165 (15), 155 (28), 128 (15), 116 (23), 104 (35), 91 (30), 78 (100). HRMS-ESI+ m/z [*M*+H]$^+$ calcd for[$C_{17}H_{15}NO_3$+H]$^+$: 282.1125, found: 282.1118.

*4.5.4. (1R, 2R, 3S, 4S, 5R, 6S, 9R, 10S, 11S, 12S, 16R, 17R)-14-Azaheptacyclo[8.6.1.0^{2,5}.0^{3,11}0^{4,9}.0^{6,17}.0^{12,16}]heptadec-7-ene-13,15-dione (**8**).*

A mixture of **7** (500 mg, 1.98 mmol) and hydroquinone (33 mg, 0.29 mmol) in a sealed tube was dissolved in xylene (50 mL). The white suspension was heated to 180 ºC for 90 hours. The yellowish suspension was allowed to cool down to room temperature and was concentrated under vacuo. The solid obtained was purified through silica by column chromatography and **8** was collected in the (DCM 99.2: MeOH) fractions as a white solid (438 mg, 44%) that was used in the next step without further purification, mp 299-300 ºC. IR ν 3230, 3073, 1975, 1945, 2903, 2735, 1773, 1698,

1359, 1342, 1290, 1229, 1175, 1149, 1064, 1019, 938, 798, 741, 706, 686, 630 cm^{-1}. ^{1}H NMR (400 MHz, $CDCl_3$) δ 1.76 (m, 2 H, 10(17)-H), 2.16 (m, 2 H, 1(11)-H), 2.33 (m, 2 H, 4(5)-H), 2.55 (m, 2 H, 6(9)-H), 2.68 (m, 2 H, 2(3)-H), 2.81 (m, 2 H, 6(9)-H), 6.22 [dd, *J* = 4.8 Hz, *J'* = 3.2 Hz, 2H, 7(8)-H], 8.0 (broad s, 1 H, NH). ^{13}C NMR (100.6 MHz, $CDCl_3$) δ: 34.3 [CH, C1(11)], 37.1 [CH, C12(16)], 37.6 [CH, C10(17)], 39.4 [CH, C2(3)], 39.5 [CH, C4(5)], 39.8 [CH, C6(9)], 130.6 [CH, C7(8)], 180.2 [C, C13(15)]. MS (GC), rt = 24.6 min, m/e (%); main ions: 253 ($M^{\cdot+}$, 47), 187 (13), 182 (12), 181 (12), 175 (26), 165 (14), 155 (26), 128 (15), 116 (22), 104 (34), 91 (27), 78 (100).

*4.5.5. (1R, 2R, 3S, 4S, 5R, 6S, 9R, 10S, 11S, 12S, 16R, 17R)-14-Azaheptacyclo[8.6.1.$0^{2,5}$.$0^{3,11}0^{4,9}$.$0^{6,17}$.$0^{12,16}$]heptadec-7-ene, hydrochloride (**9·HCl**)*

In a 3-necked round bottom flask fitted with a condenser and a thermometer, **8** (427 mg, 1.69 mmol) was added under Ar atmosphere. Dry toluene (16 mL) was then poured and Red-Al® 65% in toluene (2.60 mL, 8.43 mmol) was added dropwise. The solution was stirred at 107 ºC overnight. The solution was then allowed to cool down to room temperature and it was quenched with an aqueous 30% solution of KOH (15 mL) added dropwise. The organic phase was separated and the aqueous phase was extracted with DCM (3 x 35 mL). All the organic phases were put together, dried over anh. Na_2SO_4, filtered and concentrated under vacuo to give an orange oil (421 mg). The oil was dissolved in EtOAc and HCl/Et_2O 0.66N was added until no more precipitate was formed. The suspension was filtered under vacuo and **9·HCl** was recovered as an off-white solid (325 mg, 74%). An analytical sample was obtained by crystallization from MeOH/Et_2O, 282-283 ºC (dec.). IR ν 3041, 2918, 2902, 2726, 2602, 2484, 2376, 1594, 1395, 1373, 1347, 1300, 1255, 910, 828, 809, 685 cm^{-1}. ^{1}H NMR (400 MHz, CD_3OD) δ 1.79 [broad s, 2 H, 1(11)-H], 1.87 [m, 2 H, 10(17)-H], 2.30 [m, 2 H, 4(5)-H], 2.44 [m, 2 H, 12(16)-H], 2.54 [m, 2 H, 6(9)-H], 2.63 [m, 2 H, 2(3)-H], 3.12 [m, 2 H, 13(15)-H_a], 3.56 [m, 2 H, 13(15)-H_b], 6.27 [dd, *J* = 4.6 Hz, *J'* = 3.0 Hz, 2H, 7(8)-H]. ^{13}C NMR (100.6 MHz, CD_3OD) δ: 34.7 [CH, C12(16)], 36.7 [CH, C1(11)], 37.3 [CH, C10(17)], 39.4 [CH, C2(3)], 40.8 [CH, C4(5)], 41.2 [CH, C6(9)], 51.4 [CH_2, C13(15)], 131.9 [CH, C7(8)]. MS (DI), m/e (%); main ions: 225 ($M^{\cdot+}$, 100), 165 (9), 128 (9), 115 (16), 91 (18), 80 (22), 78 (14), 68 (49). Anal. Calcd for $C_{16}H_{19}N$·HCl·0.25 H_2O: C 72.16%, H 7.76%, Cl 13.31, N 5.26. Found: C 72.16%, H 7.74%, Cl 13.25, N 5.07.

*4.5.6. (1R, 2R, 3S, 4S, 5R, 6S, 9R, 10S, 11S, 12S, 16R, 17R)-14-Azaheptacyclo[8.6.1.$0^{2,5}$.$0^{3,11}0^{4,9}$.$0^{6,17}$.$0^{12,16}$]heptadecane, hydrochloride (**10·HCl**)*

In an roundbottom flask **9·HCl** (111 mg, 0.42 mmol) was dissolved in absolute EtOH (15 mL) and palladium on activated charcoal (235 mg, 5% in Pd) was added. The flask was fitted with a balloon filled with H_2 at atmospheric pressure and the black suspension was stirred at room temperature overnight. It was then filtered and the clear solution was concentrated under vacuo to yield **10·HCl** as a white solid (89 mg, 79%). An analytical sample was obtained by crystallization from MeOH/Et_2O, mp 292-293 ºC (dec.). IR ν 2958, 2930, 2897, 2853, 2748, 2599, 2462, 1588, 1452, 1419, 1350, 1312, 1290, 1262, 1049, 1025, 902, 825, 660 cm^{-1}. ^1H NMR (400 MHz, CD_3OD) δ: 1.43 [m, 2 H, 6(9)-H], 1.55 [m, 2 H, 7(8)-H_a], 1.63 [broad s, 2 H, 1(11)-H], 1.81 [m, 2 H, 7(8)-H_b], 2.23 [m, 2 H, 10(17)-H], 2.44 [m, 2 H, 12(16)-H], 2.57-2.65 [complex signal, 4 H, 2(3)-H and 4(5)-H], 3.19 [m, 2 H, 13(15)-H_a], 3.57 [m, 2 H, 13(15)-H_b]. ^{13}C NMR (100.6 MHz, CD_3OD) δ: 19.9 [CH_2, C7(8)], 34.7 [CH, C12(16)], 35.6 [CH, C6(9)], 36.8 [CH, C10(17)], 38.0 [CH, C1(11)], 39.9 [CH, C2(3)]*, 41.2 [CH, C4(5)]*, 51.6 [CH_2, C13(15)]. MS (GC), m/e (%); main ions: 227 ($M^{\cdot+}$, 100), 155 (5), 141 (6), 128 (8), 117 (10), 105 (5), 91 (19), 79 (11), 68 (10). Anal. Calcd for $C_{16}H_{21}N{\cdot}HCl{\cdot}0.25H_2O$: C 71.62%, H 8.45%, Cl 13.21%, N 5.22%. Found C 71.89%, H 8.49%, Cl 13.35%, N 5.00%.

*4.5.7. (1R, 2R, 3S, 4S, 5R, 6S, 9R, 10S, 11S, 12S, 16R, 17R)-14-Amidino-14-azaheptacyclo[8.6.1.$0^{2,5}$.$0^{3,11}0^{4,9}$.$0^{6,17}$.$0^{12,16}$]heptadec-7-ene, hydrochloride (**12·HCl**).*

A solution of **9·HCl** (85 mg, 0.32 mmol) in water (10 mL) was basified to pH = 14 with a 10 N aqueous solution of NaOH. It was then extracted with EtOAc (3 x 15mL) and the joined organic phase was dried over Na_2SO_4, filtered and concentrated under vacuo (yellow oil, 70 mg, 0.31 mmol, 96% yield). To a suspension of this oil in acetonitrile (3 mL), 1*H*-pyrazole-1-carboxamidine monohydrochloride (55 mg, 0.37 mmol) was added. The suspension was heated to reflux for 6 hours. The suspension was allowed to cool down to 4 ºC and left at this temperature overnight. The yellow precipitate was filtered to give **12·HCl** as an off-white solid (29 mg, 31%), mp 224-225 ºC (dec.). IR ν 3309, 3125, 2940, 1635, 1627, 1375, 1351, 1295, 1255, 1182, 1147, 1118, 1073, 828, 805, 690 cm^{-1}. ^1H NMR (400 MHz, CD_3OD) δ 1.72 [complex signal, 4

H, 10(17)-H and 1(11)-H], 2.28 [m, 2 H, 4(5)-H], 2.47-2.55 [complex signal, 4 H, 6(9) and 12(16)-H], 2.61 [m, 2 H, 2(3)-H], 3.55-3.62 [complex signal, 4 H, 13(15)-H_2], 6.25 [dd, *J* = 4.8 Hz, *J'* = 2.8 Hz, 2 H, 7(8)-H]. ^{13}C NMR (100.6 MHz, CD_3OD) δ 33.5 [CH, C12(16)], 36.4 [CH, C1(11)], 37.2 [CH, C2(3)], 37.9 [CH, C10(17)], 39.8 [CH, C4(5)], 40.0 [CH, C6(9)], 52.0 [CH_2, C13(15)], 130.5 [CH, C7(8)], 154.6 (C=NH). MS, m/e (%); main ions: 267 ($M^{\cdot+}$, 100), 266 (99), 225 (17), 224 (43), 165 (9), 117 (10), 115 (16), 91 (17), 85 (63), 78 (15), 68 (32). HRMS-ESI+ m/z [*M*+H]$^+$ calcd for [$C_{17}H_{22}N_3$+H] $^+$: 268.1808, found: 268.1811.

*4.5.8. (1R, 2R, 3S, 4S, 5R, 6S, 9R, 10S, 11S, 12S, 16R, 17R)-14-Amidino-14-azaheptacyclo[8.6.1.$0^{2,5}$.$0^{3,11}0^{4,9}$.$0^{6,17}$.$0^{12,16}$]heptadecane hydrochloride, (**11·HCl**).*

A solution of **10·HCl** (82 mg, 0.31 mmol) in water (10 mL) was basified to pH = 14 with a 10 N aqueous solution of NaOH. It was then extracted with EtOAc (3 x 15mL) and the joined organic phase was dried over Na_2SO_4, filtered and concentrated under vacuo (yellow oil, 67 mg, 0.29 mmol, 92% yield). To a suspension of this oil in acetonitrile (3 mL), 1*H*-pyrazole-1-carboxamidine monohydrochloride (52 mg, 0.29 mmol) was added. The suspension was heated to reflux for 6 hours. The suspension was allowed to cool down to 4 ºC and left at this temperature overnight. The yellow precipitate was filtered to give **11·HCl** as an off-white solid (38 mg, 42%), mp >300 ºC. IR ν 3300, 3176, 3118, 2945, 2900, 2856, 1628, 1458, 1298, 1258, 1098, 830, 729 cm^{-1}. ^{1}H NMR (400 MHz, CD_3OD) δ 1.39 [m, 2H, 6(9)-H], 1.55 [m, 4 H, 7(8)-H_a and 1(11)-H], 1.78 [m, 2 H, 7(8)-H_b], 2.10 [broad s, 2 H, 10(17)-H], 2.52 [m, 2 H, 12(16)-H], 2.60 [m, 4 H, 2(3)-H and 4(5)-H], 3.57-3.67 [complex signal, 4 H, 13(15)-H_2]. ^{13}C NMR (100.6 MHz, CD_3OD) δ 19.9 [CH_2, C7(8)], 35.0 [CH, C12(16)], 35.8 [CH, C6(9)], 37.4 [CH, C10(17)], 40.4 [CH, C2(3)]*, 40.5 [CH, C1(11)]*, 40.7 [CH, C4(5)]*, 53.6 [CH_2, C13(15)], 156.1 (C=NH). MS, m/e (%); main ions: 269 ($M^{\cdot+}$, 83), 226 (57), 141 (6), 129 (8), 117 (10), 91 (18), 85 ($C_3H_7N_3^{\cdot+}$, 100), 79 (11), 68 (11). HRMS-ESI+ m/z [*M*+H]$^+$ calcd for [$C_{17}H_{24}N_3$+H] $^+$: 270.1965, found: 273.1963.

*4.5.9. (2R, 3S, 7R, 8S, 9S, 10R)-5-Azapentacyclo[6.4.0.0^{2,10}.$0^{3,7}$.$0^{9,11}$]dodecane-4,6-dione (**17**)*

A mixture of **16** [38] (1.03 g, 4.95 mmol) and urea 99.5% (1.49 g, 24.7 mmol) was heated to 150ºC until the urea melted. Then the temperature was raised to 220ºC for 30 min. The brown paste was redissolved in water (50 mL) and DCM (50 mL). The first

organic phase was separated and the aqueous phase was extracted with DCM (5x50 mL). The combined organic phases were dried over Na_2SO_4, filtered and concentrated under reduced pressure to yield **17** as a yellow solid (737 mg, 79%), mp 211-212 ºC. IR ν 3446, 3185, 3064, 2953, 2931, 2864, 2737, 1750, 1705, 1384, 1354, 1327, 1312, 1289, 1261, 1223, 1178, 1121, 1072, 1001, 993, 936, 797, 749, 706, 650, 632, 604, 538 cm^{-1}. ^1H NMR (400 MHz, $CDCl_3$) δ 1.08 [dd, *J* = 4.8 Hz, *J'* = 0.8 Hz, 2 H, 9(10)-H, 1.26 (t, *J* = 4.8 Hz, 1 H, 11-H), 1.59 (t, *J* = 1.2 Hz, 2 H, 12-H_2), 2.11 (broad s, 1 H, 1-H), 2.45 [broad s, 2 H, 2(8)-H], 3.24 [dd, *J* = 3.2 Hz, *J'* = 2.0 Hz, 2 H, 3(7)-H], 8.40 (broad s, 1 H, NH). ^{13}C NMR (100.6 MHz, $CDCl_3$) δ 11.2 [CH, C9(10)], 12.8 (CH, C11), 31.2 (CH_2, C12), 44.2 [CH, C3(7)], 45.6 (CH, C1), 48.8 [CH, C2(8)], 179.1 [C=O, C4(6)]. MS (GC), m/e (%); main ions: 189 ($M^{\cdot+}$, 67), 118 (92), 117 [(M-$C_2H_2NO_2)^{\cdot+}$, 100], 115 (23), 92 (11), 91 (28), 65 (9), 58 (9). HRMS-ESI+ m/z $[M+H]^+$ calcd for $[C_{11}H_{11}NO_2+H]^+$: 190.0863, found: 190.0867.

*4.5.10. (2R, 3S, 7R, 8S, 9S, 10R)-5-Azapentacyclo[6.4.0.0^{2,10}.0^{3,7}.0^{9,11}]dodecane hydrochloride (**18·HCl**)*

To a solution of **17** (627 mg, 3.31 mmol) in dry toluene (22 mL) was added dropwise Red-Al® 65% in toluene (5.05 mL, 16 .57 mmol). The mixture was heated to reflux for 2 days. The black solution was quenched with KOH 30% aq. (10 mL) and the first organic phase was separated. The aqueous layer was extracted with DCM (3x20 mL) and the combined organic phases were dried over Na_2SO_4, filtered and concentrated under reduced pressure. The yellow oil was redissolved in EtOAc and HCl/Et_2O 1.2N was added until no more precipitate was formed. It was filtered under vacuo and the light brown residue was recovered as **18·HCl** (305 mg, 47%), mp 208-209 ºC. IR ν 3435, 3209, 3081, 3046, 2983, 2899, 2954, 2938, 2870, 2752, 2725, 2620, 2559, 2443, 1569, 1467, 1457, 1399, 1344, 1305, 1274, 1256, 1231, 1146, 1062, 1000, 987, 945, 890, 875, 830, 817, 770, 695, 654 cm^{-1}. ^1H NMR (400 MHz, CD_3OD) δ 1.16 [d, J = 5.2 Hz, 2 H, 9(10)-H], 1.31 (t, J = 5.2 Hz, 1 H, 11-H), 1.56 (t, J = 1.2 Hz, 2 H, 12-H_2), 2.11 (m, 1 H, 1-H), 2.13 [m, 2 H, 2(8)-H], 3.00 [dd, J = 7.2 Hz, J' = 3.2 Hz, 2 H, 3(7)-H], 3.24 [m, 2 H, 4(6)-H_a], 3.42 [dd, J = 12 Hz, J' = 3.2 Hz, 2 H, 4(6)-H_b]. ^{13}C NMR (100.6 MHz, CD_3OD) δ 11.4 [CH, C9(10)], 15.2 (CH, C11), 31.4 (CH_2, C12), 45.2 [CH, C3(7)], 46.9 (CH, C1), 47.3 [CH, C2(8)], 49.0 [CH_2, C4(6)]. MS (DI), m/e (%); main ions: 162 (10), 161 ($M^{\cdot+}$, 84), 160 (56), 132 (14), 131 (12), 129 (12), 120 (20), 118 (21), 117 (47), 116 (13), 115 (30), 107 (18), 106 (17), 95 (28), 94 (50), 93 (15), 58 (91), 83

(14), 82 (28), 81 (35), 80 (90), 79 (16), 78 (27), 78 (26), 69 (11), 68 (100), 67 (25), 65 (18), 56 (12), 51 (11). Anal. Calcd for $C_{11}H_{15}N{\cdot}HCl{\cdot}0.3H_2O{\cdot}0.15HCl$: C 63.34, H 8.09, Cl 19.55, N 6.72. Found: C 63.30, H 8.04, Cl 19.78, N 6.71.

*4.5.11. (2R, 3S, 7R, 8S, 9S, 10R)-5-Amidino-5-azapentacyclo[6.4.0.0^{2,10}.0^{3,7}.0^{9,11}]dodecane hydrochloride (**19·HCl**)*

A mixture of **18·HCl** (305 mg, 1.54 mmol), 1*H*-pyrazole-1-carboxamidine monohydrochloride (271 mg, 1.85 mmol) and triethylamine (0.4 mL, 2.78 mmol) was dissolved in acetonitrile (12 mL). The yellow suspension was heated to mild reflux for 6 hours. The suspension was allowed to cool down a bit and the flask was sealed and left at 4 ºC overnight. The yellow liquid phase was poured out from the flask and **19·HCl** was recovered as a light orange solid (258 mg, 70%). An analytical sample was crystallized from isopropanol, mp 153-154 ºC. IR ν 3567, 3482, 3344, 3304, 3190, 3138, 3066, 2995, 2958, 2945, 2881, 2861, 2677, 1627, 1508, 1467, 1458, 1367, 1342, 1304, 1284, 1249, 1225, 1189, 1160, 1073, 1036, 957, 937, 832, 802, 787, 775, 644, 582 cm^{-1}. ^{1}H NMR (400 MHz, CD_3OD) δ 1.00 [dd, *J* = 5.2, *J'* = 0.8 Hz, 2 H, 9(10)-H], 1.20 (t, *J* = 5.2 Hz, 1 H, 11-H), 1.55 (t, *J* = 1.2 Hz, 2 H, 12-H_2), 2.02 (broad s, 1 H, 1-H), 2.13 [broad s, 2 H, 2(8)-H], 2.97 [m, 2 H, 3(7)-H], 3.39 [m, 2 H, 4(6)-H_a], 3.65 [dd, *J* = 10.8 Hz, *J'* = 1.2 Hz, 2 H, 4(6)-H_b]. ^{13}C NMR (100.6 MHz, CD_3OD) δ 10.7 [CH, C9(10)], 13.9 (CH, C11), 31.5 (CH_2, C12), 44.8 [CH, C3(7)], 45.9 (CH, C1), 48.5 [CH, C2(8)], 50.1 [CH_2, C4(6)], 155.7 [C=NH]. MS (DI), m/e (%); main ions: 204 (15), 203 ($M^{\cdot+}$, 100), 202 (13), 160 (49), 137 (13), 131 (10), 129 (28), 128 (14), 124 (19), 117 (25), 116 (12), 115 (26), 111 (39), 110 (97), 95 (11), 94 (21), 93 (12), 91 (49), 85 (51), 82 (17), 80 (24), 79 (14), 78 (15), 77 (23), 72 (20), 68 (68), 67 (14), 65 (16). Anal. Calcd for $C_{12}H_{17}N_3{\cdot}HCl{\cdot}0.75H_2O{\cdot}0.05HCl$: C 56.50, H 7.73, Cl 14.59, N 16.47. Found: C 56.55, H 7.59, Cl 14.49, N16.62.

4.6. Molecular modeling

4.6.1. Molecular dynamics simulations

The binding mode of compounds **9** and **10** to the wt M2 channel and its V27A variant embedded on a model bilayer of 1-palmitoyl-2-oleoyl-sn-glycero-3-phosphocholine (POPC) was studied by MD simulations. The M2 channel was modeled from the solid state NMR structure obtained by Sharma et al. (PDB entry 2L0J) [45], and it was oriented using as template the solid state NMR structure with PDB entry 2KQT [40] as deposited in the Orientations of Proteins in Membranes (OPM) database

[46]. The X-ray crystallographic structure 3LBW [47] from the Protein Data Bank was used to model the position of water molecules inside the channel. The initial position of the ligand was chosen to resemble the orientation of Amt in the 2KQT structure.

The CHARMM-GUI [48] web server was used to build up the initial systems. Briefly, the complex formed by the protein, the inner lumen water molecules, and the ligand was embedded on a 100 Å × 100 Å POPC bilayer patch. A 25 Å layer of TIP3P [49] water molecules was set up at both sides of the bilayer, and K^+ cations and $Cl^–$ anions were added to achieve an ionic strength of 150 mM. The Parm99SB [50] force field was used for the protein, the ligands were parametrized using the gaff [51] force field in conjunction with RESP HF/6-31G(d) charges as implemented in the Antechamber module of AMBER12 software package [52], and the POPC molecules were parametrized according to the gaff-lipid11 force field [53]. Joung and Cheatham parameters were used to model the counterions [54]. Each system comprised around 97000 atoms, including the protein ligand complex, 265 POPC molecules, around 58000 waters and 108 (51 K^+; 57 $Cl^–$) counterions in a simulation box of 100000 $Å^3$.

The geometry of the system was minimized in five cycles that combined 3500 steps of steepest descent algorithm followed by 4500 of conjugate gradient. Thermalization of the system was performed in 5 steps of 1 ns, where the temperature was gradually increased from 50 K to 298 K, while the protein, ligand, and POPC molecules were restrained with a force constant of 1 kcal $mol^{–1}$ $Å^{–2}$. Prior to the production runs, a set of 20 ns MD simulations was performed to smoothly equilibrate the systems by gradually reducing the restraints first for the POPC molecules (restraints reduced by 0.1 kcal $mol^{–1}$ $Å^{–2}$ at each step) and then for the protein (restraints reduced by 0.2 kcal $mol^{–1}$ $Å^{–2}$ at each step). At this point, three different replicas were generated for each ligand–protein complex (accounting for a total of 12 different simulation systems).

We took advantage of the GPU-accelerated PMEMD module from AMBER12 software package for the production runs, which consisted of 50 ns trajectories (accounting for a global simulation time of 600 ns) using SHAKE for bonds involving hydrogen atoms, a time step of 2 fs, periodic boundary conditions using anisotropic constant pressure and temperature (298 K; Langevin thermostat with a collision frequency of 3 $ps^{–1}$), particle mesh Ewald for long-range electrostatic interactions, and a

cutoff of 10 Å for nonbonded interactions. The analysis of the trajectories was performed for snapshots taken every 5 ps.

4.6.2. Log P calculation

The octanol/water partition coefficient (log P) of Amt and compounds **9**-**12** was determined by means of QM calculations at B3LYP/6-31G(d) basis set. We first optimized the structure of each compound in their neutral state in gas phase, and then a single-point calculation was performed in water and octanol using the B3LYP-parametrized version of the IEF/MST continuum solvation model [55]. Calculations were performed using a locally modified version of Gaussian09 [56].

Acknowledgments

M.R.-C. acknowledges a predoctoral grant from the Government of Andorra (ATCR2012/2013-00XX-AND). J.J.-J. and S.V. thank the Spanish Ministerio de Ciencia e Innovación (FIS fellowship to J.J.-J. and grant CTQ2011-22433 to S.V.; grant SAF2014-57094-R) and the Generalitat de Catalunya (FI fellowship to S.L.; grant 2014SGR1189) for financial support. L.N. acknowledges financial support from the Geconcerteerde Onderzoeksacties (GOA/15/019/TBA), and the technical assistance from W. van Dam. F.J.L is grateful to Icrea Academia for financial support. The Barcelona Supercomputer Center is acknowledged for computational facilities.

References

[1] Molinari, N.-A. M.; Ortega-Sanchez, I. R.; Messonnier, M. L.; Thompson, W. W.; Wortley, P. M.; Weintraub, E.; Bridges, C. B. The annual impact of seasonal influenza in the US: Measuring disease burden and costs. *Vaccine* **2007**, *25*, 5086–5096.

[2] Hay, A J.; Gregory, V.; Douglas, a R.; Lin, Y. P. The evolution of human influenza viruses. *Philos. Trans. R. Soc. Lond. B. Biol. Sci.* **2001**, *356*, 1861–1870.

[3] Reid, A. H.; Taubenberger, J. K.; Fanning, T. G. The 1918 Spanish influenza: Integrating history and biology. *Microbes Infect.* **2001**, *3*, 81–87.

[4] Taubenberger, J. K.; Morens, D. M. 1918 Influenza: The mother of all pandemics. *Emerg. Infect. Dis.* **2006**, *12*, 15–22.

[5] Neumann, G.; Noda, T.; Kawaoka, Y. Emergence and pandemic potential of swine-origin H1N1 influenza virus. *Nature* **2009**, *459*, 931–939.

[6] Cohen, J.; Enserink, M. After delays, WHO agrees: the 2009 pandemic has begun. *Science* **2009**, *324*, 1496–1497.

[7] Michaelis, M.; Doerr, H. W.; Cinatl, J. Novel swine-origin influenza A virus in humans: Another pandemic knocking at the door. *Med. Microbiol. Immunol.* **2009**, *198*, 175–183.

[8] Dawood, F. S.; Iuliano, A. D.; Reed, C.; Meltzer, M. I.; Shay, D. K.; Cheng, P.-Y.; Bandaranayake, D.; Breiman, R. F.; Brooks, W. A.; Buchy, P.; Feikin, D. R.; Fowler, K. B.; Gordon, A.; Hien, N. T.; Horby, P.; Huang, Q. S.; Katz, M. A.; Krishnan, A.; Lal, R.; Montgomery, J. M.; Mølbak, K.; Pebody, R.; Presanis, A. M.; Razuri, H.; Steens, A.; Tinoco, Y. O.; Wallinga, J.; Yu, H.; Vong, S.; Bresee, J.; Widdowson, M.-A. Estimated global mortality associated with the first 12 months of 2009 pandemic influenza A H1N1 virus circulation: A modelling study. *Lancet Infect. Dis.* **2012**, *12*, 687–695.

[9] Abdel-Ghafar, A.; Chotpitayasunondh, T.; Zhancheng, G.; Hayden, F.; Hien, N.; de Jong, M.; Naghdaliyev, A.; Peiris, J.; Shindo, N.; Soeroso, S.; Uyeki, T. Update on avian influenza A (H5N1) virus infection in humans. *N Engl J Med* **2008**, *358*, 261–273.

[10] Yu, H.; Cowling, B. J.; Feng, L.; Lau, E. H. Y.; Liao, Q.; Tsang, T. K.; Peng, Z.; Wu, P.; Liu, F.; Fang, V. J.; Zhang, H.; Li, M.; Zeng, L.; Xu, Z.; Li, Z.; Luo, H.; Li, Q.; Feng, Z.; Cao, B.; Yang, W.; Wu, J. T.; Wang, Y.; Leung, G. M. Human infection with avian influenza A H7N9 virus: An assessment of clinical severity. *Lancet* **2013**, *382*, 138–145.

[11] Lee, S. M.-Y.; Yen, H.-L. Targeting the host or the virus: Current and novel concepts for antiviral approaches against influenza virus infection. *Antiviral Res.* **2012**, *96*, 391–404.

[12] Vanderlinden, E.; Naesens, L. Emerging Antiviral Strategies to Interfere with Influenza Virus Entry. *Med. Res. Rev.* **2014**, *34*, 301–339.

[13] Bright, R. A.; Shay, D. K.; Shu, B.; Cox, N. J.; Klimov, A. I. Adamantane resistance among influenza A viruses isolated early during the 2005-2006 influenza season in the United States. *JAMA* **2006**, *295*, 891–894.

[14] Hayden, F. G.; de Jong, M. D. Emerging Influenza Antiviral Resistance Threats. *J. Infect. Dis.* **2011**, *203*, 6–10.

[15] Fiore, A. E.; Fry, A. M.; Shay, D. K.; Gubareva, L. V.; Bresee, J. S.; Uyeki, T. M. Antiviral agents for the treatment and chemoprophylaxis of influenza - recommendations of the Advisory Committee on Immunization Practices (ACIP). *MMWR Recomm. Rep.* **2011**, *60*, 1–28.

[16] Moscona, A. Global transmission of oseltamivir-resistant influenza. *N Engl J Med* **2009**, *360*, 953–956.

[17] Baz, M. M.; Abed, Y.; Papenburg, J.; Bouhy, X.; Hamelin, M.-E.; Boivin, G. Emergence of Oseltamivir-Resistant Pandemic H1N1 Virus during Prophylaxis. *N. Engl. J. Med.* **2009**, *361*, 2296–2297.

[18] Sheu, T. G.; Fry, A. M.; Garten, R. J.; Deyde, V. M.; Shwe, T.; Bullion, L.; Peebles, P. J.; Li, Y.; Klimov, A. I.; Gubareva, L. V. Dual resistance to adamantanes and oseltamivir among seasonal influenza A(H1N1) viruses: 2008-2010. *J. Infect. Dis.* **2011**, *203*, 13–17.

[19] Pinto, L. H.; Lamb, R. A. The M2 proton channels of influenza A and B viruses. *J. Biol. Chem.* **2006**, *281*, 8997–9000.

[20] Pinto, L. H.; Holsinger, L. J.; Lamb, R. A. Influenza virus M2 protein has ion channel activity. *Cell* **1992**, *69*, 517–528.

[21] Takeuchi, K.; Lamb, R. A. Influenza virus M2 protein ion channel activity stabilizes the native form of fowl plague virus hemagglutinin during intracellular transport. *J. Virol.* **1994**, *68*, 911–919.

[22] Grambas, S.; Hay, A. J. Maturation of influenza A virus hemagglutinin - Estimates of the pH encountered during transport and its regulation by the M2 protein. *Virology* **1992**, *190*, 11–18.

[23] Balannik, V.; Carnevale, V.; Fiorin, G.; Levine, B. G.; Lamb, R. A.; Klein, M. L.; Degrado, W. F.; Pinto, L. H. Functional studies and modeling of pore-lining residue mutants of the influenza A virus M2 ion channel. *Biochemistry* **2010**, *49*, 696–708.

[24] Suzuki, H.; Saito, R.; Masuda, H.; Oshitani, H.; Sato, M.; Sato, I. Emergence of amantadine-resistant influenza A viruses: Epidemiological study. *J. Infect. Chemother.* **2003**, *9*, 195–200.

[25] Furuse, Y.; Suzuki, A.; Oshitani, H. Large-scale sequence analysis of M gene of influenza A viruses from different species: Mechanisms for emergence and spread of amantadine resistance. *Antimicrob. Agents Chemother.* **2009**, *53*, 4457–4463.

[26] Bright, R. A.; Medina, M.; Xu, X.; Perez-Oronoz, G.; Wallis, T. R.; Davis, X. M.; Povinelli, L.; Cox, N. J.; Klimov, A. I. Incidence of adamantane resistance among

influenza A (H3N2) viruses isolated worldwide from 1994 to 2005: A cause for concern. *Lancet* **2005**, *366*, 1175–1181.

[27] Saito, R.; Sakai, T.; Sato, I.; Sano, Y.; Oshitani, H.; Sato, M.; Suzuki, H. Frequency of amantadine-resistant influenza A viruses during two seasons featuring cocirculation of H1N1 and H3N2. *J. Clin. Microbiol.* **2003**, *41*, 2164–2165.

[28] Wu, Y.; Canturk, B.; Jo, H.; Ma, C.; Gianti, E.; Fiorin, G.; Pinto, L. H.; Lamb, R. A.; Klein, M. L.; Wang, J.; DeGrado, W. F. Discovery of Dual Inhibitors That Bind in Different Orientations to the Wild-Type versus the Amantadine-Resistant S31N Mutant of the Influenza A Virus M2 Proton Channel. *J. Am. Chem. Soc.* **2014**, *136*, 17987–17995.

[29] Rey-Carrizo, M.; Torres, E.; Ma, C.; Barniol-Xicota, M.; Wang, J.; Wu, Y.; Naesens, L.; Degrado, W. F.; Lamb, R. A.; Pinto, L. H.; Vazquez, S. Azatetracyclo[5.2.1.$1^{5,8}$.$0^{1,5}$]undecane derivatives: from wild-type inhibitors of the M2 ion channel of influenza A virus to derivatives with potent activity against the V27A mutant. *J. Med. Chem.* **2013**, *56*, 9265–9274.

[30] Rey-Carrizo, M.; Barniol-Xicota, M.; Ma, C.; Frigolé-Vivas, M.; Torres, E.; Naesens, L.; Llabrés, S.; Juárez-Jiménez, J.; Luque, F. J.; DeGrado, W. F.; Lamb, R. A.; Pinto, L. H.; Vázquez, S. Easily Accessible Polycyclic Amines that Inhibit the Wild-Type and Amantadine-Resistant Mutants of the M2 Channel of Influenza A Virus. *J. Med. Chem.* **2014**, *57*, 5738–5747.

[31] Camps, P.; Duque, M. D.; Vázquez, S.; Naesens, L.; De Clercq, E.; Sureda, F. X.; López-Querol, M.; Camins, A.; Pallàs, M.; Prathalingam, S. R.; Kelly, J. M.; Romero, V.; Ivorra, D.; Cortés, D. Synthesis and pharmacological evaluation of several ring-contracted amantadine analogs. *Bioorg. Med. Chem.* **2008**, *16*, 9925–9936.

[32] Duque, M. D.; Ma, C.; Torres, E.; Wang, J.; Naesens, L.; Juárez-Jiménez, J.; Camps, P.; Luque, F. J.; DeGrado, W. F.; Lamb, R. A.; Pinto, L. H.; Vázquez, S. Exploring the Size Limit of Templates for Inhibitors of the M2 Ion Channel of Influenza A Virus. *J. Med. Chem.* **2011**, *54*, 2646–2657.

[33] Torres, E.; Fernández, R.; Miquet, S.; Font-Bardia, M.; Vanderlinden, E.; Naesens, L.; Vázquez, S. Synthesis and anti-influenza A virus activity of 2,2-dialkylamantadines and related compounds. *ACS Med. Chem. Lett.* **2012**, *3*, 1065–1069.

[34] Torres, E.; Duque, M. D.; Vanderlinden, E.; Ma, C.; Pinto, L. H.; Camps, P.; Froeyen, M.; Vázquez, S.; Naesens, L. Role of the viral hemagglutinin in the anti-

influenza virus activity of newly synthesized polycyclic amine compounds. *Antiviral Res.* **2013**, *99*, 281–291.

[35] Abou-Gharbia, M.; Patel, U. R.; Webb, M. B.; Moyer, J. A.; Andree, T. H.; Muth, E. A. Polycyclic aryl- and heteroarylpiperazinyl imides as 5-HT1A receptor ligands and potential anxiolytic agents: synthesis and structure-activity relationship studies. *J. Med. Chem.* **1988**, *31*, 1382–1392.

[36] Srikrishna, A. Synthesis of hexacyclo[6.5.1.$0^{2,7}$.$0^{3,11}$.$0^{4,9}$.$0^{10,14}$]tetradeca-5,12-diene *Synth. Commun.* **1990**, *20*, 279–284.

[37] Forman, M. A.; Moran, C.; Herres, J. P.; Stairs, J.; Chopko, E.; Pozzessere, A.; Kerrigan, M.; Kelly, C.; Lowchyj, L.; Salandria, K.; Gallo, A.; Loutzenhiser, E. Generation & rxns pentacyclo[4.3.0.$0^{2,4}$.$0^{3,8}$.$0^{5,7}$]non-4-ene. *J. Org. Chem.* **2007**, *72*, 2996–3005.

[38] Russell, G. A.; Holland, G. W.; Chang, K.; Robert, G. K.; Chung, C. S. C.; Stanley, K.; Schmitt, K.; Blankespoor, R.; Kosugi, Y. Aliphatic semidiones. XXV. Bicyclo[n.2.1]alkane-2,3-semidiones. *J. Am. Chem. Soc.* **1974**, *96*, 7237–7248.

[39] CCDC XXXXX.

[40] Cady, S.D; Schmidt-Rohr, K; Wang, J; Soto, C.S.; DeGrado, W.F.; Hong, M. Structure of the amantadine binding site of influenza M2 proton channels in lipid bilayers. *Nature* **2010**, *463*, 689-92.

[41] Stevaert, A.; Dallocchio, R.; Dessì, A.; Pala, N.; Rogolino, D.; Sechi, M.; Naesens, L. Mutational analysis of the binding pockets of the diketo acid inhibitor L-742,001 in the influenza virus PA endonuclease. *J. Virol.* **2013**, *87*, 10524-10538.

[42] Gazzarrini, S.; Kang, M.; Abenavoli, A.; Romani, G.; Olivari, G.; Gaslini, D.; Ferrara, G.; Van Etten, J. L.; Kreim, M.; Kast, S. M.; Thiel, G.; Moroni, A. Chlorella virus ATCV-1 encodes a functional potassium channel of 82 amino acids. *Biochem. J.* **2009**, *420*, 295-303.

[43] Balannik, V.; Lamb, R. A.; Pinto, L. H. The oligomeric state of the active BM2 ion channel protein of influenza B virus. *J. Biol. Chem.* **2008**, *283*, 4895-4904.

[44] Vanderlinden E.; Göktas F.; Cesur Z.; Froeyen M.; Reed M. L.; Russell, C. J.; Cesur, N.; Naesens L. Novel inhibitors of influenza virus fusion: structure-activity relationship and interaction with the viral hemagglutinin. *J. Virol.* **2010**, *84*, 4277-4288.

[45] Sharma, M.; Yi, M.; Dong, H.; Qin, H.; Peterson, E.; Busath, D.D.; Zhou, H.X.; Cross, T.A. Insight into the mechanism of the influenza A proton channel from a structure in a lipid bilayer. *Science* **2010,** *330*, 509-512.

[46] Lomize, M.A.; Lomize, A.L.; Pogozheva, I.D.; Mosberg, H.I. (2006) OPM: Orientations of Proteins in Membranes database. *Bioinformatics* **2006**, *22*, 623-625.

[47] Acharya, R.; Carnevale, V.; Florin, G.; Levine, B.G.; Polishchuk, A.L.; Balannik, V.; Samish, I.; Lamb, R.A., Pinto, L.H., DeGrado, W.F.; Klein, M.L. Structure and mechanism of proton transport through the transmembrane tetrameric M2 protein bundle of the influenza A virus. *Proc. Natl Acad. Sci. U. S. A.* **2010**, *107*, 15075-15080.

[48] Jo, S.; Kim, T.; Iyer, V.G.; Im W. CHARMM-GUI: A Web-based Graphical User Interface for CHARMM. *J. Comput. Chem.* **2008,** *29*, 1859-1865.

[49] Mark, P.; Nilsson, L. Structure and dynamics of the TIP3P, SPC, and SPC/E water models at 298 K. *J. Phys Chem. A* **2001**, *105*, 9954-9960.

[50] Hornak, V.; Abel, R.; Okur, A.; Strockbine, B.; Roitberg, A.; Simmerling, C. Comparison of multiple Amber force fields and development of improved protein backbone parameters. *Proteins*, **2006**, *65*, 712-725.

[51] Wang, J.M.; Wolf, R.M.; Caldwell, J.W.; Kollman, P.A.; Case, D.A. Development and testing of a general amber force field. *J. Comput. Chem.* **2005**, 26, 1157-1174.

[52] Case, D. A.; Darden, T. A.; Cheatham, III, T. E.; Simmerling, C. L.; Wang, J.; Duke, R.E.; Luo, R.; Walker, R. C.; Zhang, W.; Merz, K. M.; Roberts, B.; Hayik, S.; Roitberg, A.; Seabra, G.; Swails, J.; Goetz, A. W.; Kolossváry, I.; Wong, K. F.; Paesani, F.; Vanicek, J.; Wolf, R. M.; Liu, J.; Wu, X.; Brozell, S. R.; Steinbrecher, T.; Gohlke, H.; Cai, Q.; Ye, X.; Wang, J.; Hsieh, M.-J.; Cui, G.; Roe, D. R.; Mathews, D. H.; Seetin, M. G.; Salomon- Ferrer, R.; Sagui, C.; Babin, V.; Luchko, T.; Gusarov, S.; Kovalenko, A.; Kollman, P. A. (2012), *AMBER 12*, University of California, San Francisco.

[53] Dickson, C. J.; Rosso, L.; Betz, R. M.; Walker, R. C.; Gould, I. R. GAFFlipid: a General Amber Force Field for the accurate molecular dynamics simulation of phospholipid, *Soft Matter* **2012**, *8*, 9617-9627.

[54] Joung, I. S.; Cheatham, T. E. Determination of alkali and halide monovalent ion parameters for use in explicitly solvated biomolecular simulations, *J. Phys. Chem. B.* **2008**, *112*, 9020–9041.

[55] Curutchet, C.; Orozco, M.; Luque, F. J. Solvation in octanol: parametrization of the continuum MST model, *J. Comput. Chem.* **2001**, *22*, 1180–1193.

[56] Frisch, M. J.; Trucks, G. W.; Schlegel, H. B.; Scuseria, G. E.; Robb, M. A.; Cheeseman, J. R. et al., Gaussian 09, Revision B.01, Gaussian 09, Revis. B.01, Gaussian, Inc., Wallingford CT. (2009)

LEGENDS FOR FIGURES AND SCHEMES

Figure 1. **Structures of amantadine, rimantadine and some reported compounds with potent activities against the wt, S31N and/or V27A mutants**[a]

[a]The IC_{50} values shown correspond to the 50% inhibitory concentrations determined by TEVC assay. The inhibition percentages shown were determined at 100 µM for 2 min by TEVC [28,29]. N.T: Not Tested.

Scheme 1. **Synthesis of new polycyclic amines 9 and 10 and guanidine derivatives 11 and 12**

a: sealed tube, neat, 140 ºC, overnight (89%); b: sodium, liquid NH_3, dry THF, dry MeOH, -60 ºC, 30 min; c: HCl 10%, water, room temperature, 1h (41 % overall); d: hydroquinone, sealed tube, xylene, 180 ºC, 90h (44% overall); e: Vitride, dry toluene, reflux, overnight (74%); f: H_2, 1atm, Pd/C, absolute EtOH, room temperature, overnight (79%); g: 1*H*-pyrazole-1-carboxamidine, Et_3N, ACN, reflux, 6h (42% for **11**, 31% for **12**).

Scheme 2. Mechanism of the one-pot decarbonylation coupled with intramolecular Diels-Alder reaction of 7

Figure 2. **Crystal structure (ORTEP) of 18·HCl. Thermal ellipsoids shown at 50% probability**

Figure 3. **Representation of the predicted binding mode of compounds 9 and 10** (shown as orange and yellow sticks, respectively) to the interior of the wt M2 channel and its V27A variant. The side chains of pore-lining residues are shown and labelled.

Scheme3. Synthesis of the second family of compounds including amine 18 and guanidine 19

a: H_2, 400 psi, Pd/C, absolute EtOH, room temperature, 2 days (90%); b: urea, neat, 150 ºC then 200 ºC, 30 min (79%); c: vitride, dry toluene, reflux, 2 days (47%); d: 1*H*-pyrazole-1-carboxamidine, Et_3N, ACN, reflux, 6h (70%).

Table 1. Inhibitory effect of the synthesized compounds on proton channel function[a] **of wt, S31N or V27A mutant A/M2 proteins**

[a] Isochronic (2 min) values for IC_{50} are given. See text and experimental section for further details. [b]ND: Not Determined.

Table 2. Antiviral activity in influenza virus-infected MDCK[a] cells.
[a]MDCK: Madin-Darby canine kidney cells; virus strains: A/PR/8/34 (A/H1N1) and A/HK/7/87 (A/H3N2). [b]50% effective concentration, or compound concentration producing 50% inhibition of virus replication, as determined by microscopic scoring of the CPE at 72 h post infection, or by the MTS cell viability test. [c]EC_{50}: concentration at which the plaque number is reduced by 50% compared to untreated virus control in the virus plaque reduction assay (PRA). [d]EC_{99}: compound concentration giving 2-log_{10} reduction in virus yield, as determined by quantifying the virus in the supernatant at 24 h post infection, using an RT-qPCR based virus yield assay [41]. [e]CC_{50}: 50% cytotoxic concentration, as determined by the MTS cell viability test. [f]MCC: minimum cytotoxic concentration, or concentration producing minimal alterations in cell morphology after 72 h incubation with compound. Values shown are the mean of 2-3 determinations.

Figure 4. **Activity of the compounds in an influenza virus plaque reduction assay.** MDCK cells were infected with influenza virus (strain A/HK/7/87; 25 PFU per well) in the presence of the test compounds. After 72 h incubation, plaques were visualized by crystal violet staining. VC: mock-treated virus control; CC: uninfected cell control.

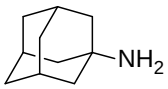

amantadine
A/M2 wt IC_{50} = 16.1 μM (% inh. = 91%)
A/M2 V27A IC_{50} > 500 μM (% inh. = 11%)
A/M2 S31N IC_{50} = 200 μM (% inh. = 36%)

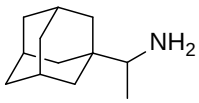

rimantadine
A/M2 wt IC_{50} = 10.8 μM
A/M2 V27A IC_{50} > 500 μM
A/M2 S31N IC_{50} > 500 μM

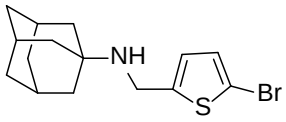

1
A/M2 % inh. wt = 77 %
A/M2 % inh. V27A = N.T.
A/M2 % inh. S31N = 76%

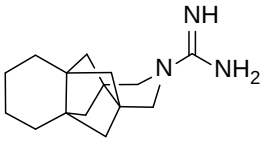

2
A/M2 wt IC_{50} = 3 μM
A/M2 V27A IC_{50} = 0.29 μM
A/M2 S31N IC_{50} > 100 μM

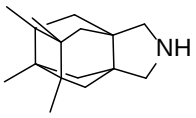

3
A/M2 wt IC_{50} = 18.0 μM
A/M2 V27A IC_{50} = 0.70 μM
A/M2 S31N IC_{50} > 100 μM
A/M2 L26FIC_{50} = 8.6 μM

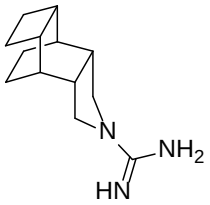

4
A/M2 wt IC_{50} = 2.1 μM
A/M2 V27A IC_{50} = 22.6 μM
A/M2 S31N IC_{50} > 100 μM

Figure 1.

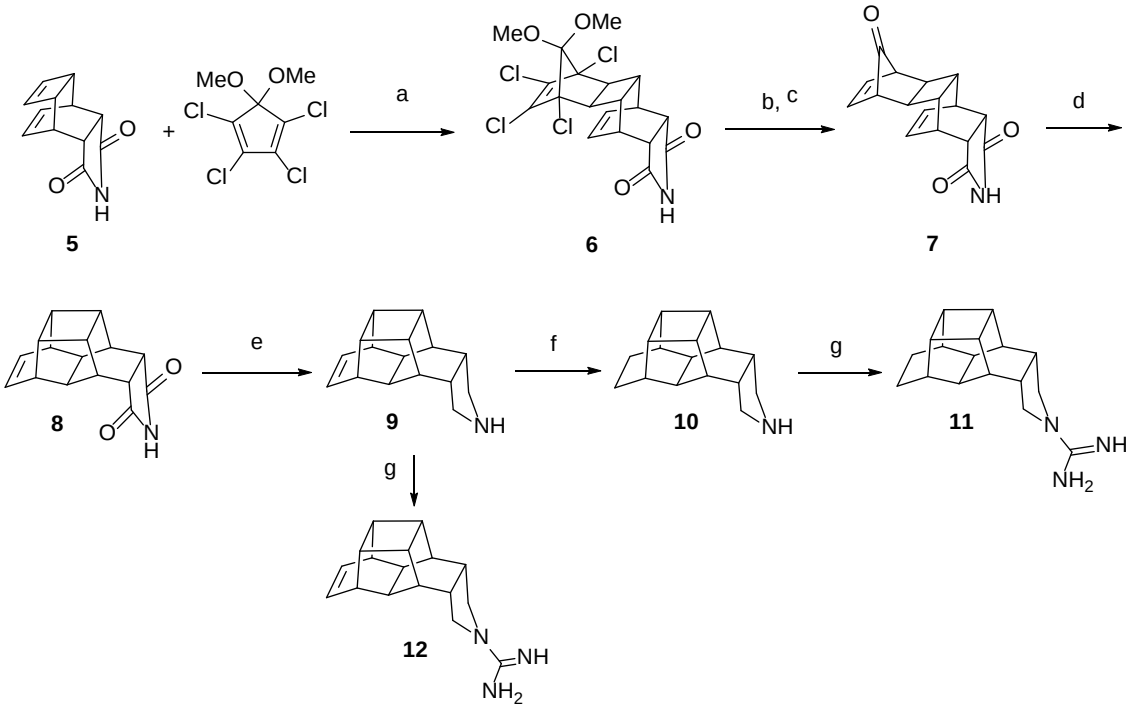

Scheme 1.

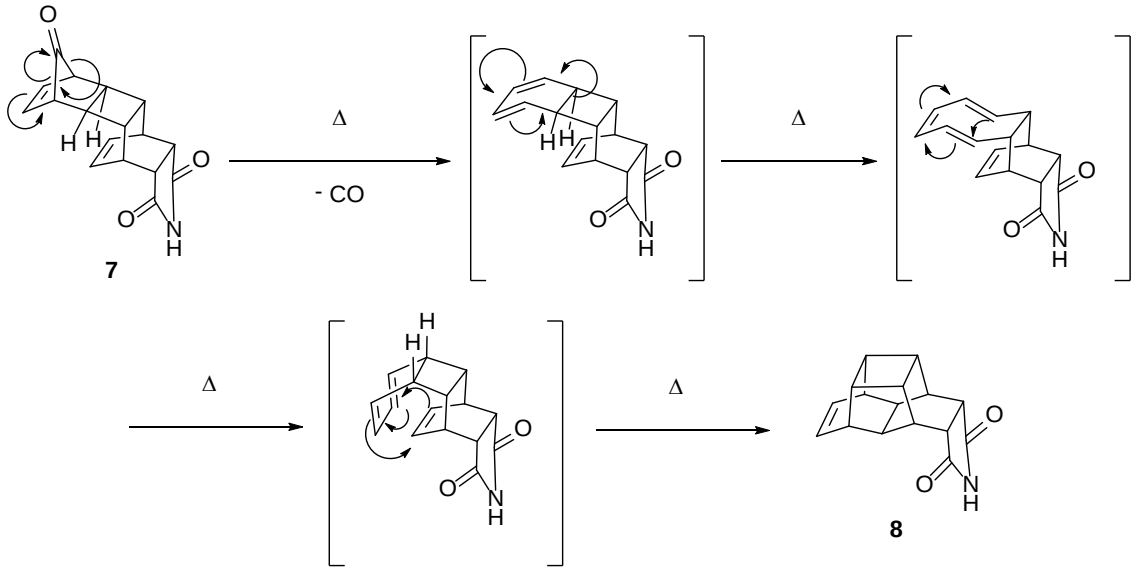

Scheme 2

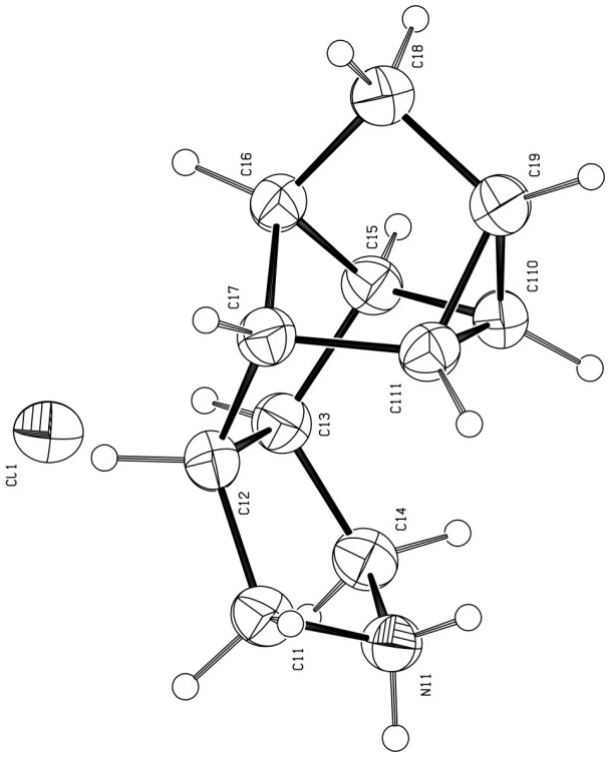

Figure 2.

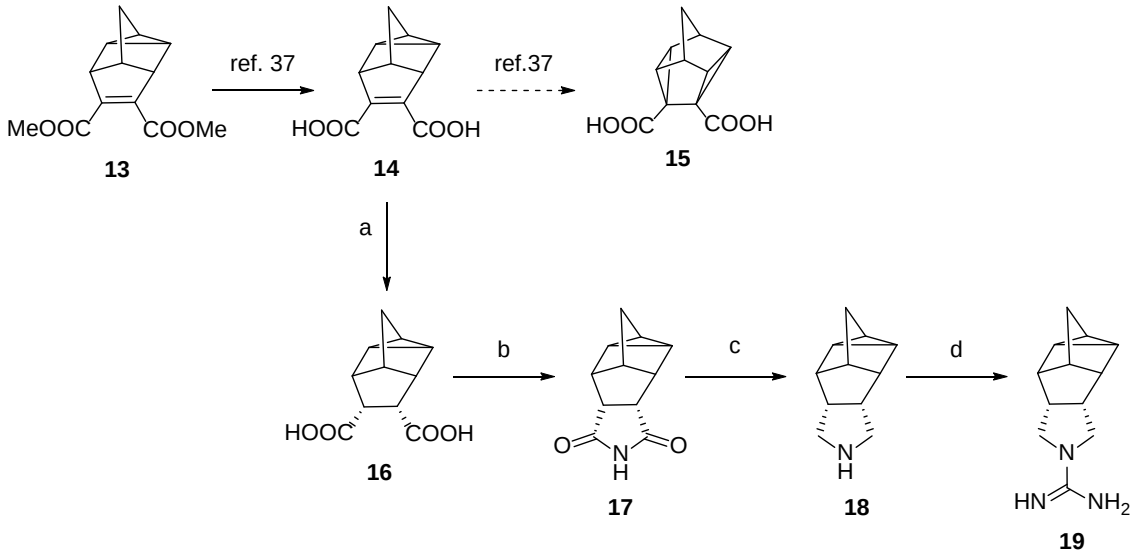
MeOOC
COOMe
13
ref. 37
HOOC
COOH
14
ref.37
HOOC
COOH
15
a
HOOC
COOH
16
b
O
N
H
O
17
c
N
H
18
d
N
HN
NH2
19

Scheme 3.

	A/M2 *wt* (mean ± SE)		**A/M2 S31N** (mean ± SE)		**A/M2 V27A** (mean ± SE)	
Compound	Inhibition by 100 μM for 2 min (%)	IC_{50} (μM)	Inhibition by 100 μM for 2 min (%)	IC_{50} (μM)	Inhibition by 100 μM for 2 min (%)	IC_{50} (μM)
Amantadine	91.0 ± 2.1	16.0 ± 1.2	35.6 ± 1.5	199.9 ± 13.5	10.8 ± 2.0	ND[b]
4	94.5 ± 1.6	2.1	2.6 ± 1.4	ND	75.9 ± 1.2	22.6
9	96.4 ± 1.3	2.6	0	ND	49.0 ± 2.8	ND
10	98.1 ± 0.5	2.1	0	ND	83.9 ± 0.7	17.2
11	90.6 ± 3.1	3.7	4.7 ± 0.7	ND	71.2 ± 3.9	32.2
12	89.6 ± 0.9	6.9	0	ND	54.0 ± 0.6	ND
18	93.7 ± 0.8	3.3	0	ND	0	ND
19	99.0 ± 0.5	0.84	2.0 ± 1.1	ND	0	ND

Table 1.

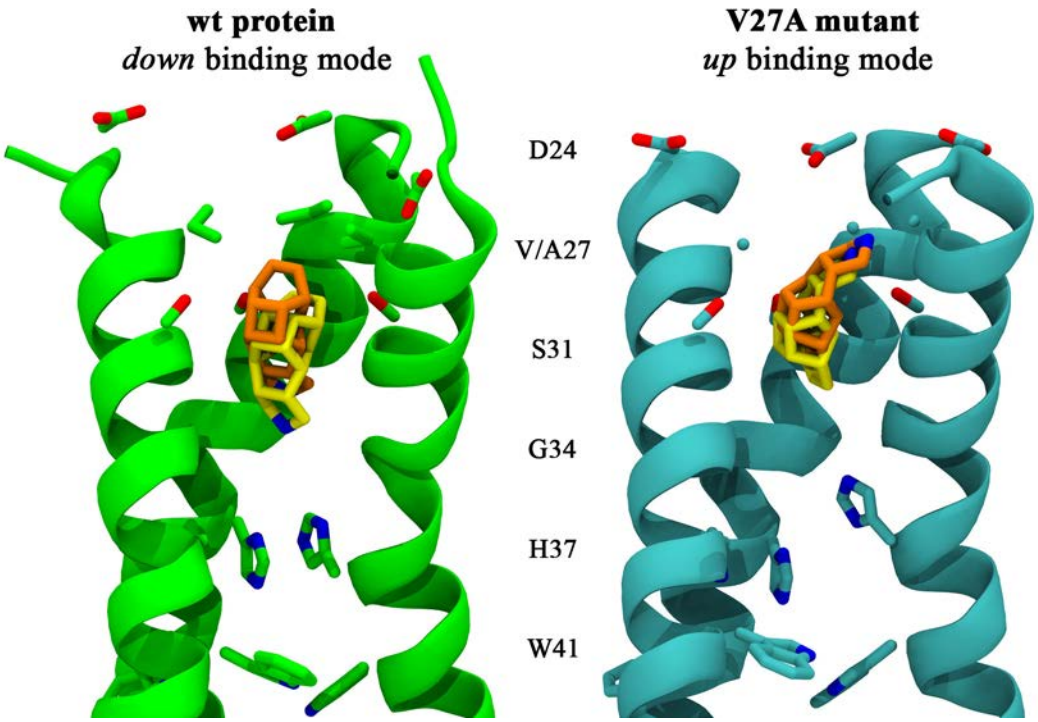
wt protein
down binding mode
V27A mutant
up binding mode
D24
V/A27
S31
G34
H37
W41

Figure 3.

	Antiviral activity (μM)						Cytotoxicity (μM)	
	A/PR/8/34		A/HK/7/87					
Compound	EC_{50} (CPE)[b]	EC_{50} (MTS)[b]	EC_{50} (CPE)[b]	EC_{50} (MTS)[b]	EC_{50} (PRA)[c]	EC_{99} (Yield)[d]	CC_{50}[e]	MCC[f]
9	>100	>100	>100	>100	0.37	3.45	11	20
10	>100	>100	>100	>100	0.54	>2	3.7	4.0
11	>100	>100	>100	>100	>5	>2	4.6	7.0
12	>100	>100	>100	>100	>5	>2	1.2	2.0
18	>100	>100	>100	>100	6.7	28	>100	>100
19	>100	>100	>100	>100	>100	>50	50	>100
Amantadine	30	34	1.4	1.4	0.14	0.72	>500	≥500
Rimantadine	7.6	5.1	0.81	0.15	0.02	1.77	230	500

Table 2.

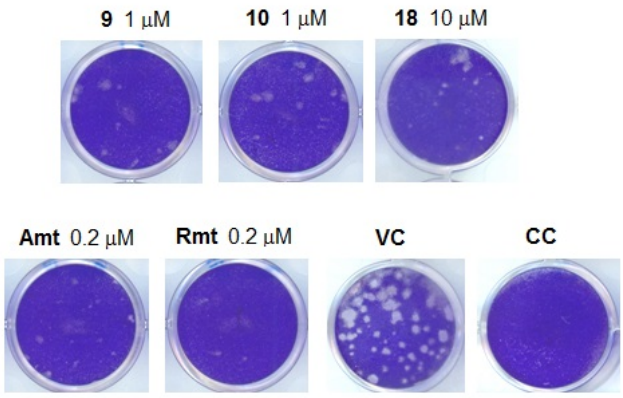

Figure 4.

Supporting Information

New polycyclic amine inhibitors of influenza A virus: unexpected binding mode in the V27A mutant M2 channel

Matias Rey-Carrizo[a], Sabrina Gazzarrini[b], Marta Frigolé-Vivas[a], Salomé Llabrés[c], Jordi Juárez-Jiménez[c], Mercè Font-Bardia[d], Lieve Naesens[e], Anna Moroni[b], Francisco J. Luque[c], and Santiago Vázquez[a,*]

Table of contents

X-Ray crystallographic data

Crystal structure report for **18·HCl**

A prismatic crystal of $C_{12}H_{17}N_3 \cdot HCl$ (0.1x0.1x0.2 mm) was selected and mounted on a MAR345 diffractometer with an image plate detector. Unit-cell parameters were determined from 783 reflections ($3 < \theta < 31^o$) and refined by least-squares method. Intensities were collected with graphite monochromatized Mo Kα radiation, using φ scan-technique.15743 reflections were measured in the range $1.53 \leq \theta \leq 30.93$. 2695 of which were non-equivalent by symmetry (Rint(on I) = 0.030). 2478 reflections were assumed as observed applying the condition $I > 2\ \sigma(I)$. Lorentz-polarization and absorption corrections were made.

The structure was solved by Direct methods, using SHELXS computer program (Sheldrick, G.M., (1997), Crystallogr. 2008, A64, 112) and refined by full-matrix least-squares method with SHELX97 computer program (Sheldrick, G.M., (1997), Crystallogr. 2008, A64, 112), using 126 reflections, (very negative intensities were not assumed). The function minimized was $\Sigma\ w\ ||Fo|^2 - |Fc|^2\ |^2$, where $w = [\sigma^2(I) + (0.0339P)^2+1.5332P]^{-1}$, and $P = (|Fo|^2 + 2\ |Fc|^2\ )/3$, f, f' and f'' were taken from International Tables of X-Ray Crystallography (International Tables of X-Ray Crystallography, (1974), Ed. Kynoch press, Vol. IV, pp 99-100 and 149).

2H atoms were located from a difference synthesis and refined with isotropic temperature factor and 14H atoms were computed and refined, using a riding model, with isotropic temperature factor equal to 1.2 time the equivalent temperature factor of the atom which are linked. The final R(on F) factor was 0.040, wR(on $|F|^2$) = 0.098 and goodness of fit = 1.162 for all observed reflections. Number of refined parameters was 126. Max. shift/esd = 0.00, Mean shift/esd = 0.00. Max. and min. peaks in final difference synthesis was 0.138 and -0.168 $eÅ^{-3}$, respectively.

Figure S1. Selected geometrical parameters (distances in Å; tilt angle in degrees) for the binding of compound **9** to the wt M2 channel along the trajectories sampled for the three 50 ns MD replicas. Left: Distance from the amine N to the His37 plane and tilt angle (defined as the angle between amine N, COM of ligand, and COM of His37 Cα atoms). Right: Distances from the COM of ligand to the plane formed by tetrads of residues along the pore.

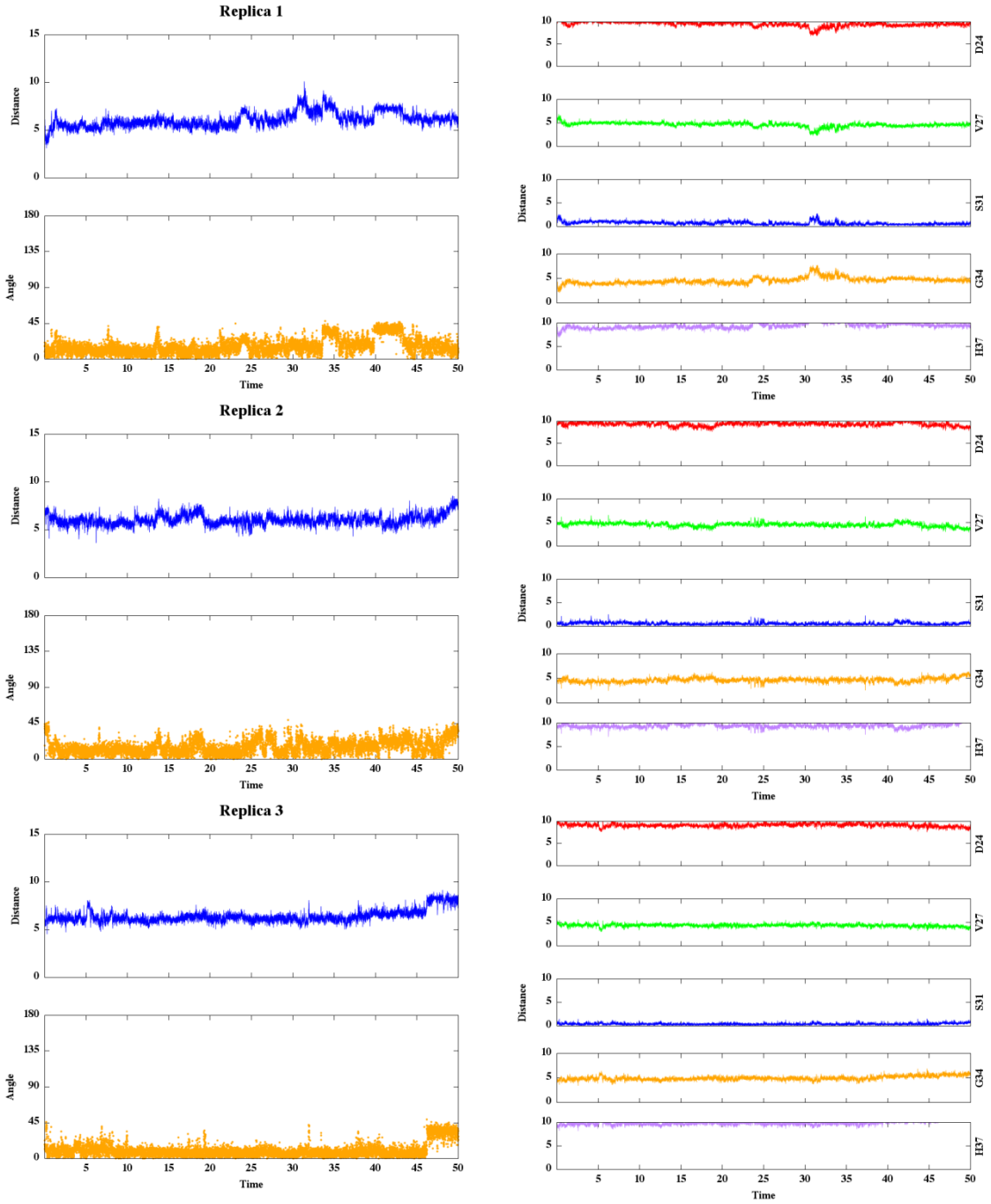

Figure S2. Selected geometrical parameters (distances in Å; tilt angle in degrees) for the binding of compound **9** to the V27A mutant M2 channel along the trajectories sampled for the three 50 ns MD replicas. Left: Distance from the amine N to the His37 plane and tilt angle (defined as the angle between amine N, COM of ligand, and COM of His37 Cα atoms). Right: Distances from the COM of ligand to the plane formed by tetrads of residues along the pore.

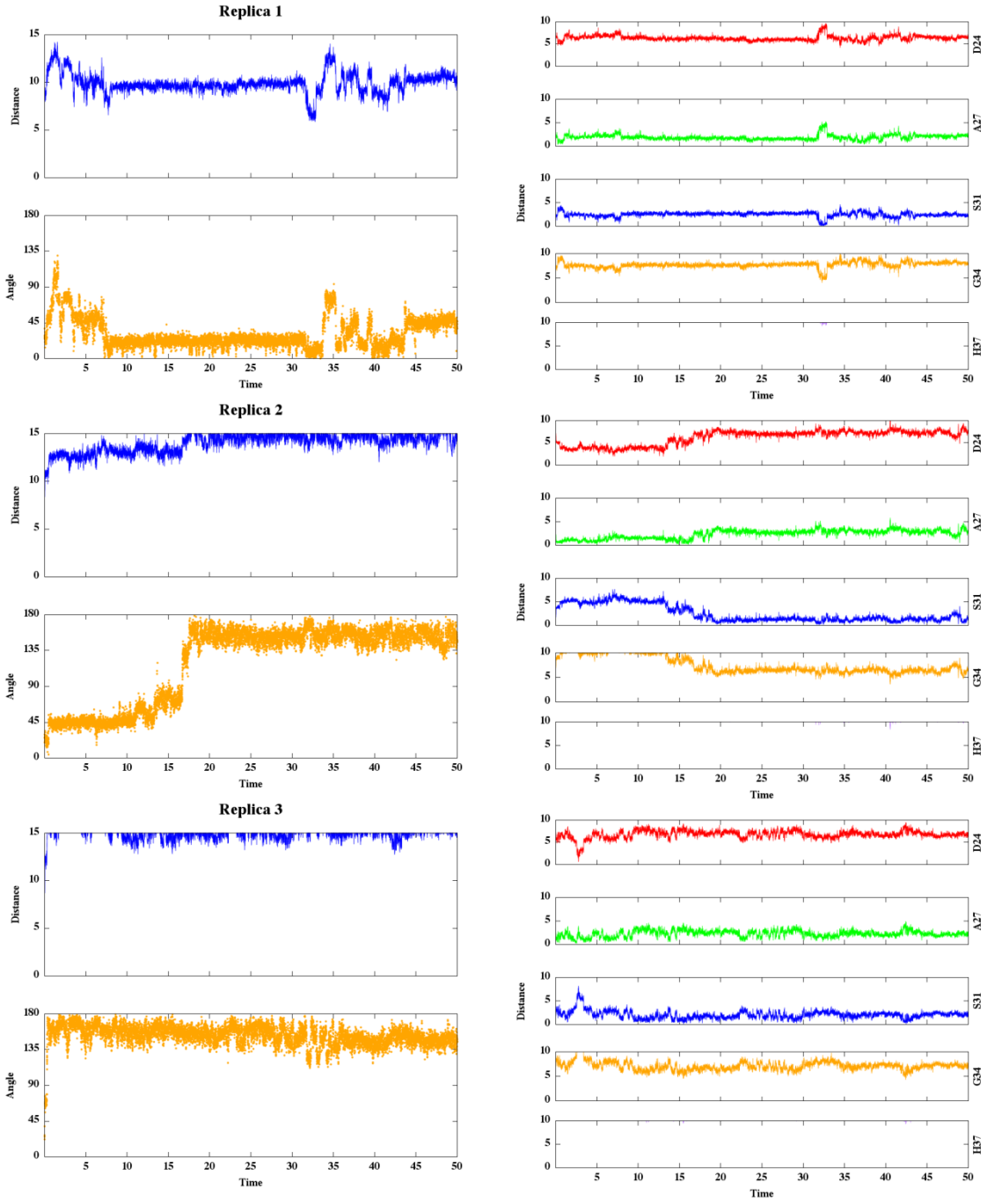

Figure S3. Selected geometrical parameters (distances in Å; tilt angle in degrees) for the binding of compound **10** to the wt M2 channel along the trajectories sampled for the three 50 ns MD replicas. Left: Distance from the amine N to the His37 plane and tilt angle (defined as the angle between amine N, COM of ligand, and COM of His37 Cα atoms). Right: Distances from the COM of ligand to the plane formed by tetrads of residues along the pore.

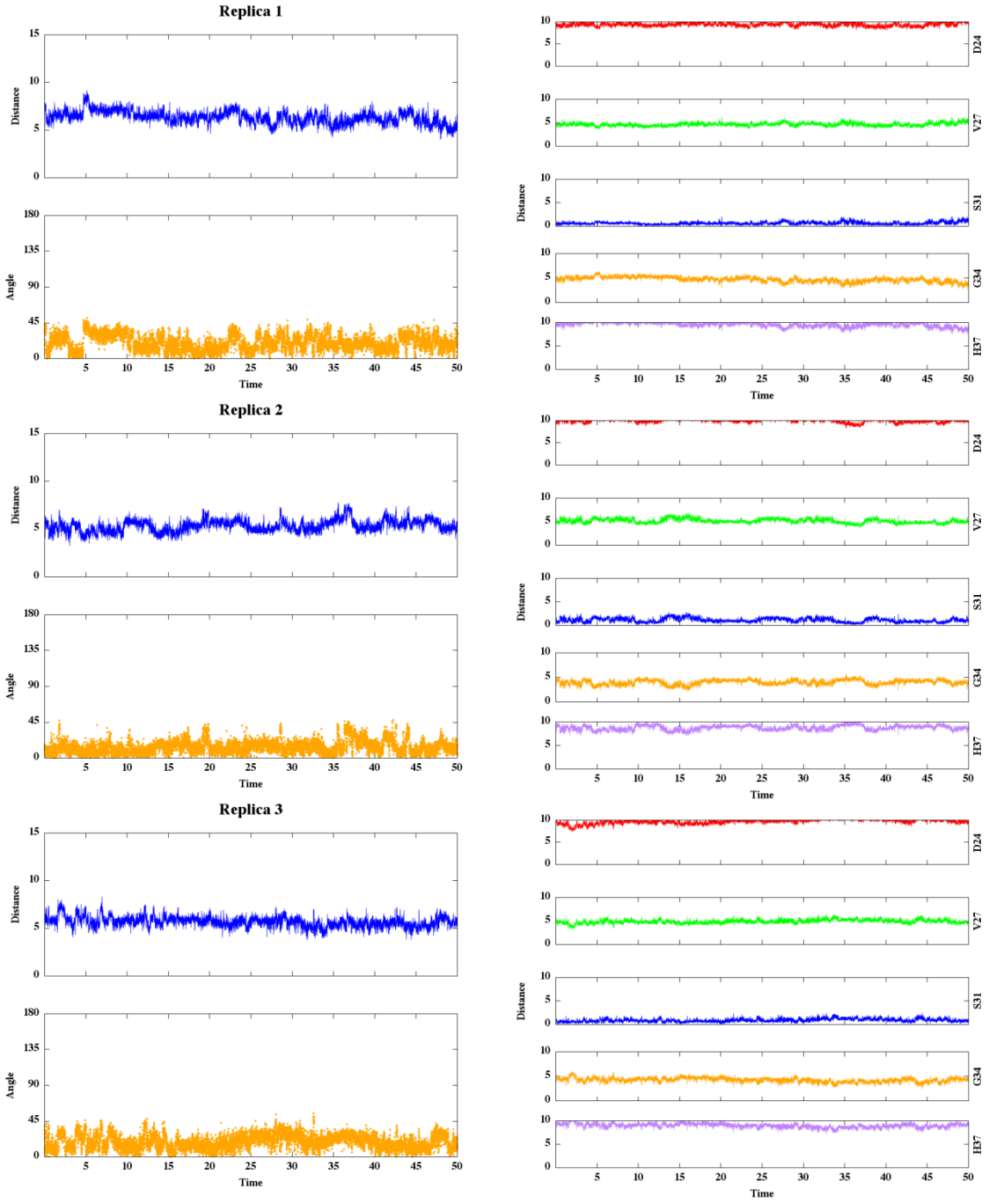

Figure S4. Selected geometrical parameters (distances in Å; tilt angle in degrees) for the binding of compound **10** to the V27A mutant M2 channel along the trajectories sampled for the three 50 ns MD replicas. Left: Distance from the amine N to the His37 plane and tilt angle (defined as the angle between amine N, COM of ligand, and COM of His37 Cα atoms). Right: Distances from the COM of ligand to the plane formed by tetrads of residues along the pore.

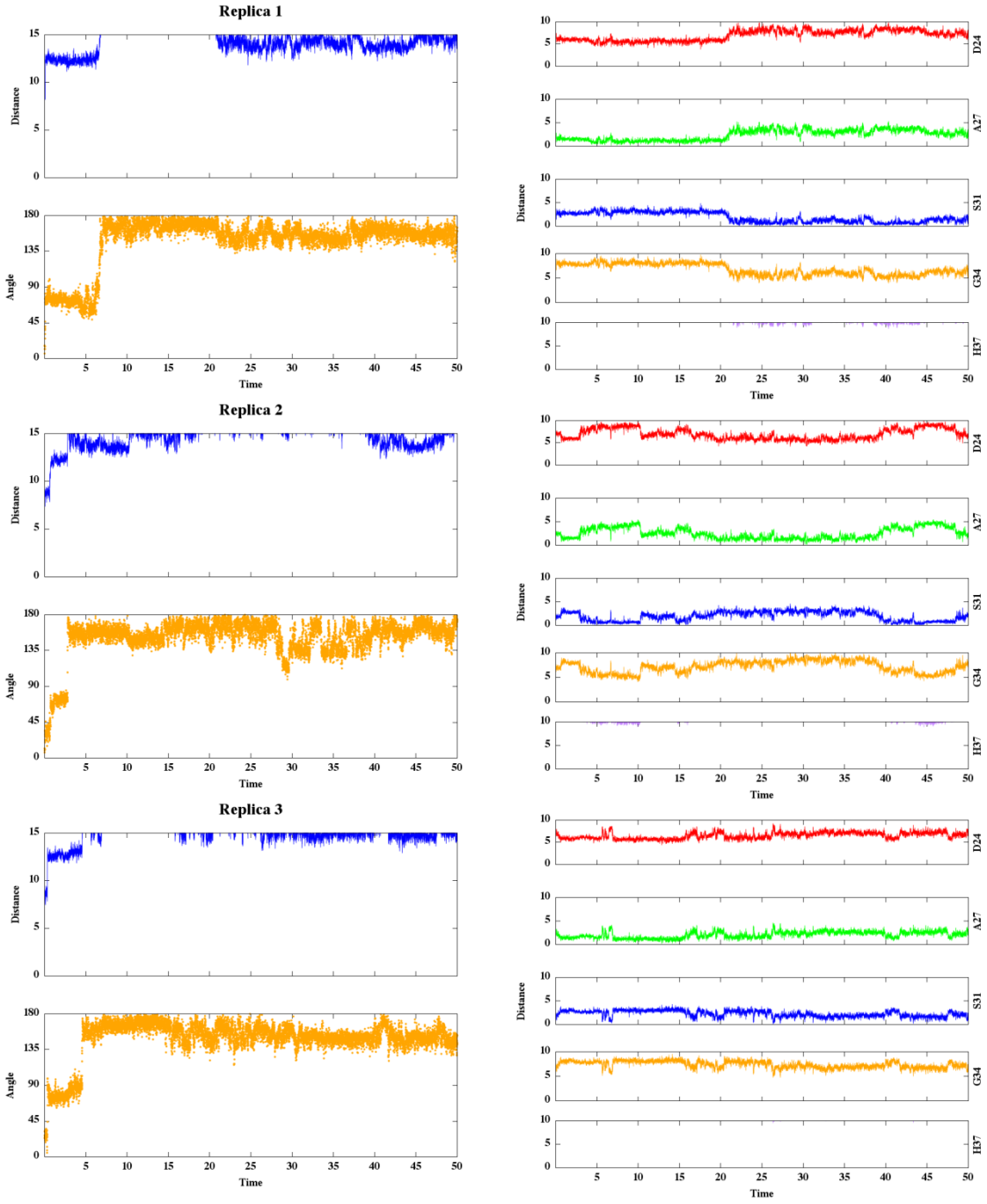

^{1}H NMR (400 MHz, $CDCl_3$) **6**

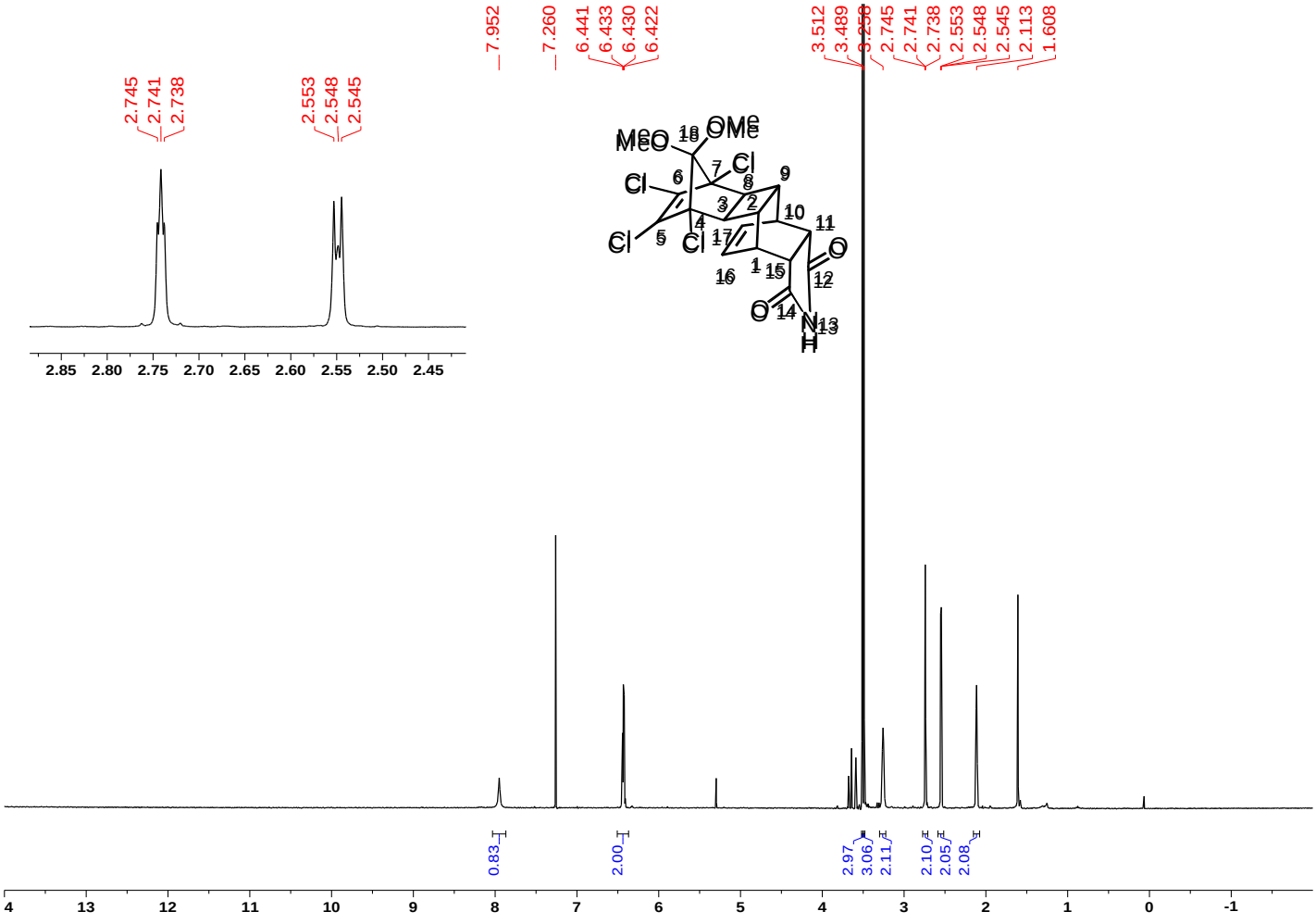

^{13}C NMR (100.6 MHz, $CDCl_3$) **6**

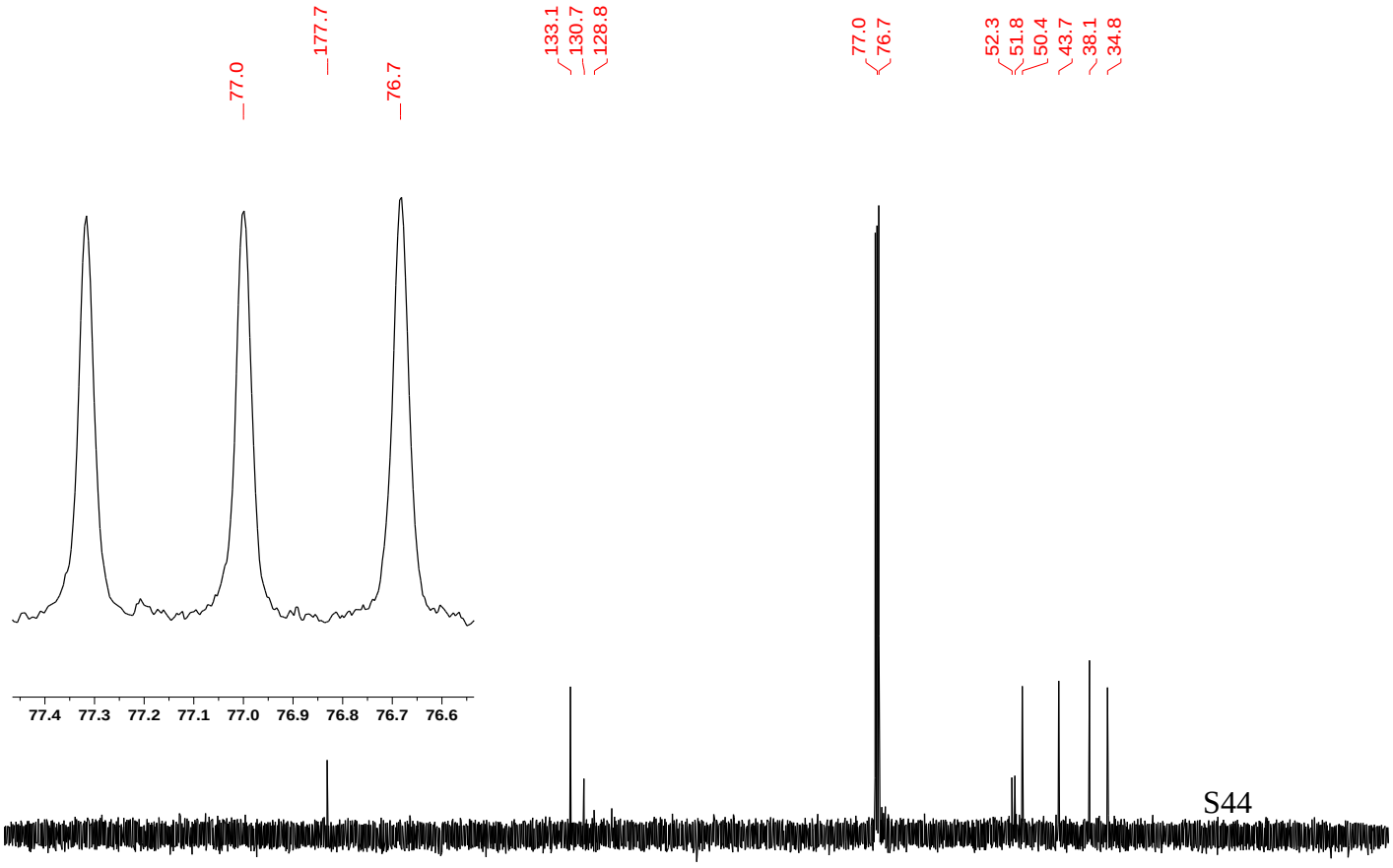

^{1}H NMR (400 MHz, $CDCl_3$) **7**

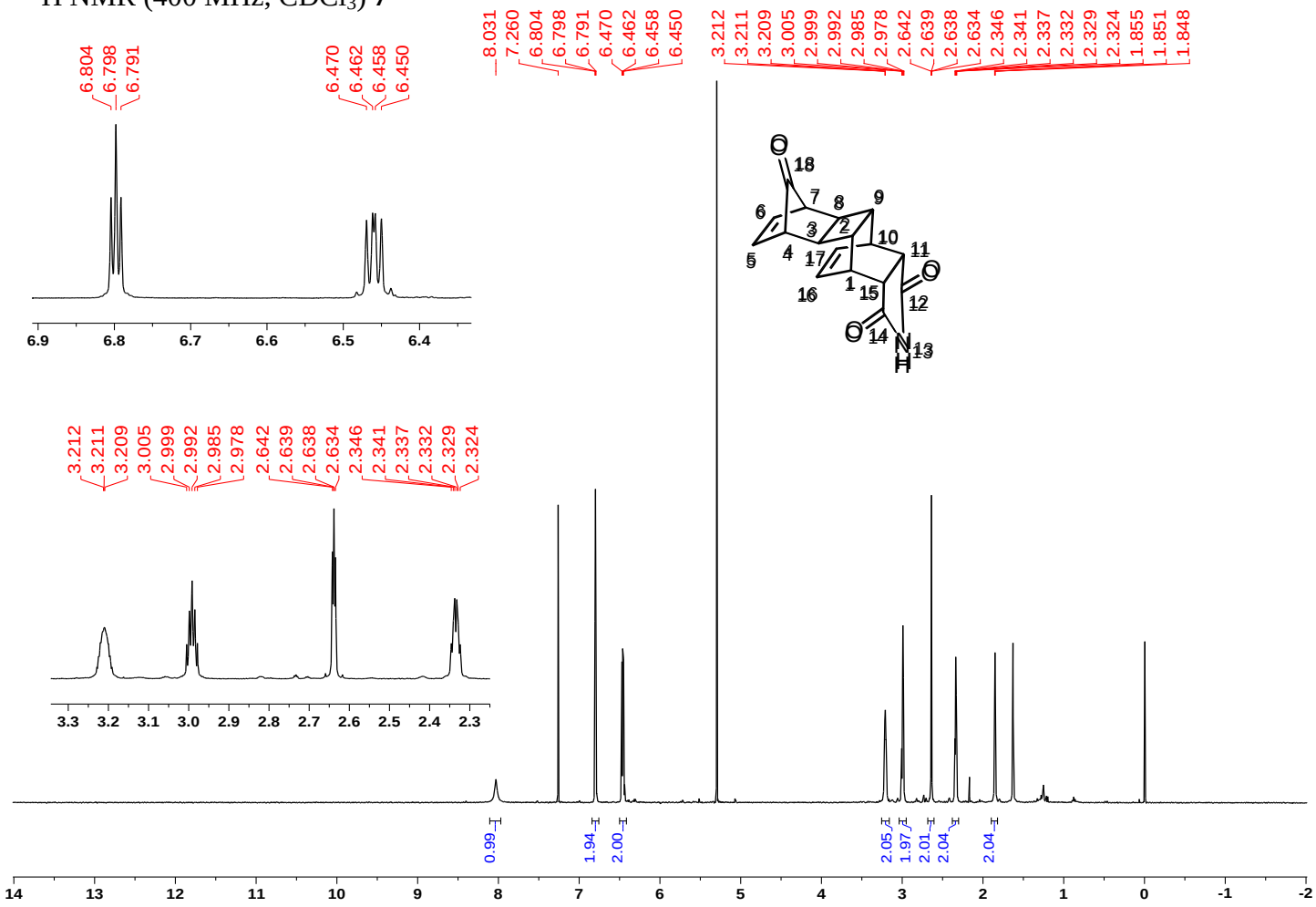

^{13}C NMR (100.6 MHz, $CDCl_3$) **7**

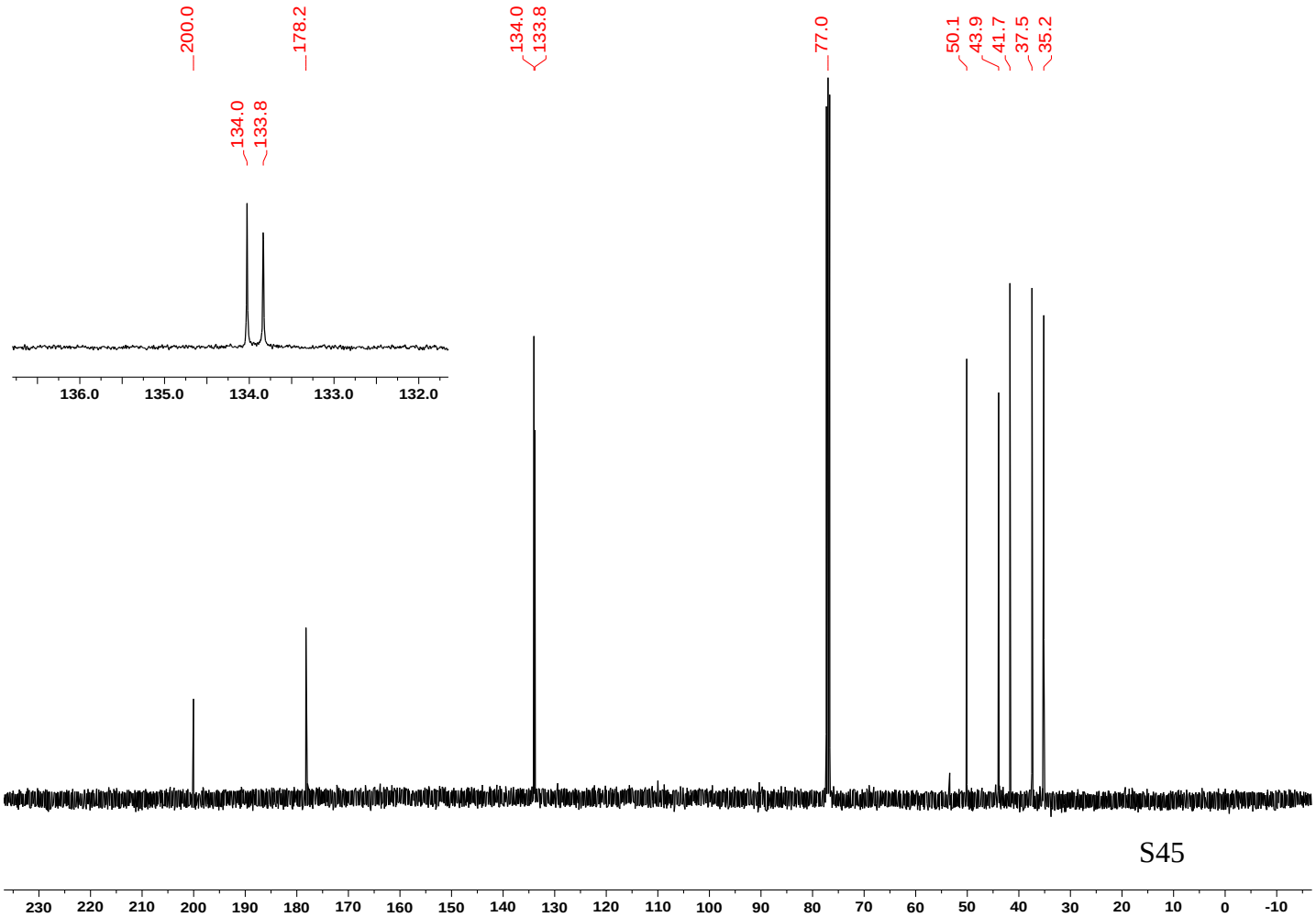

^{1}H NMR (400 MHz, $CDCl_3$) **8**

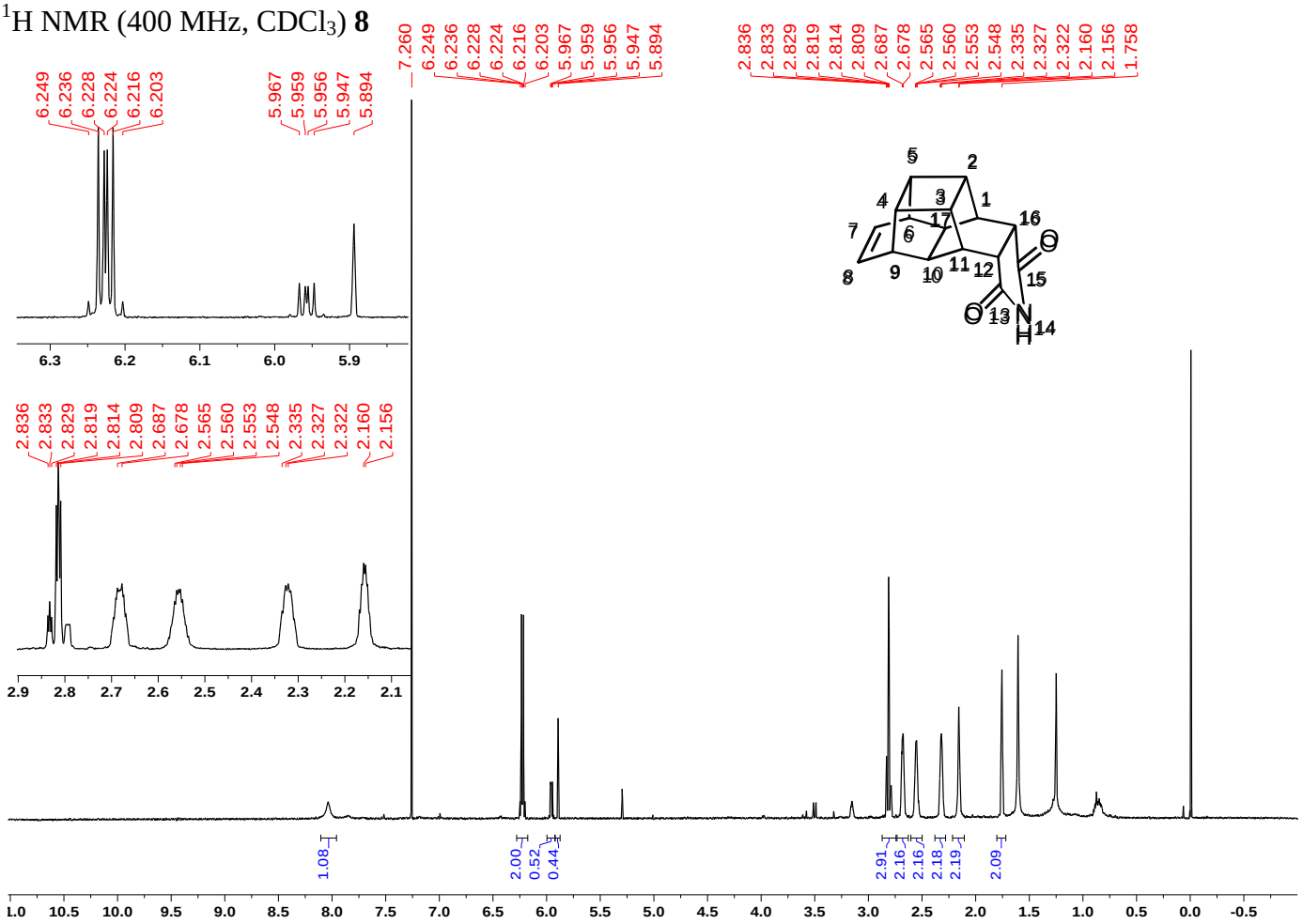

^{13}C NMR (100.6 MHz, $CDCl_3$) **8**

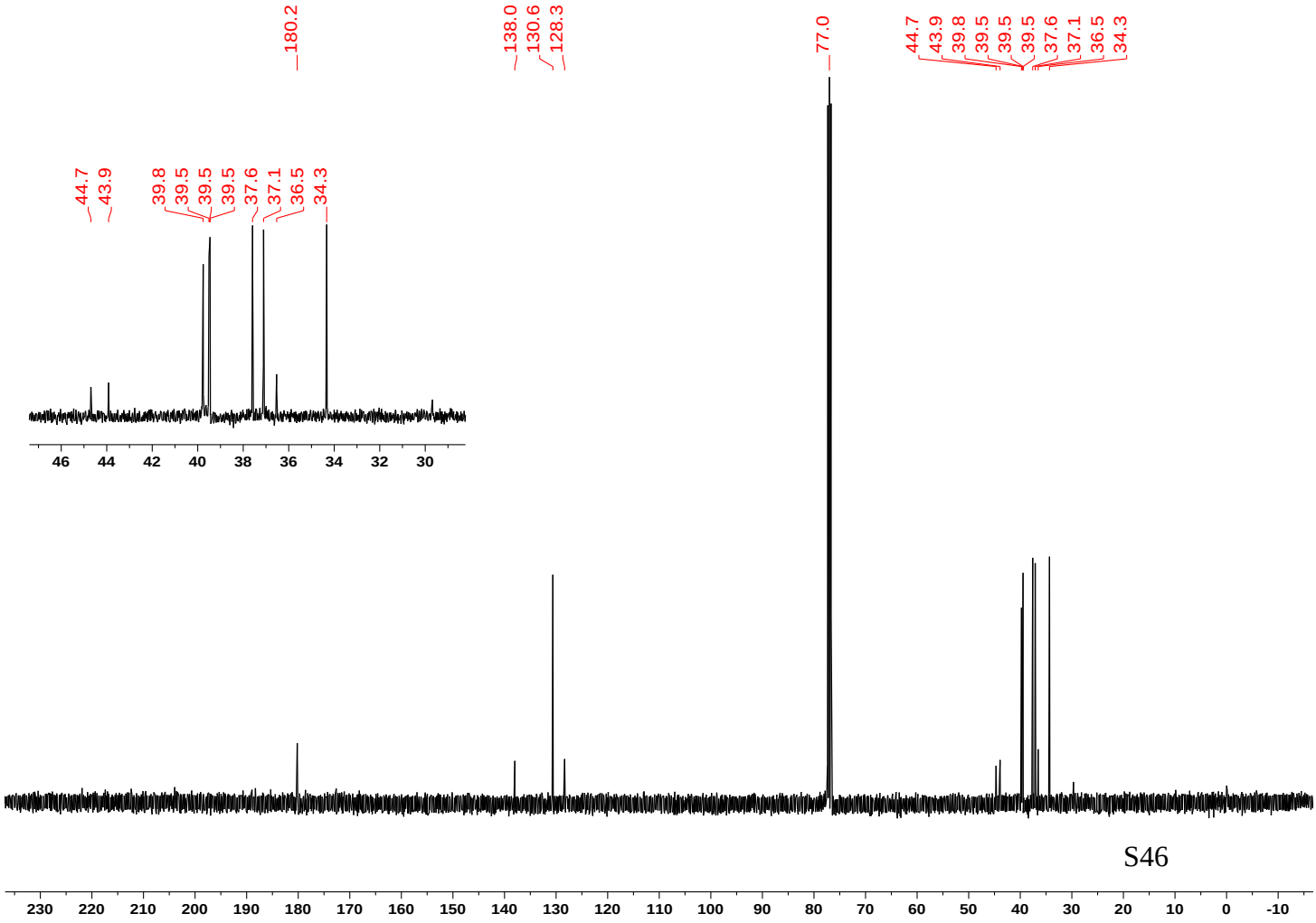

^{1}H NMR (400 MHz, CD_3OD) **9·HCl**

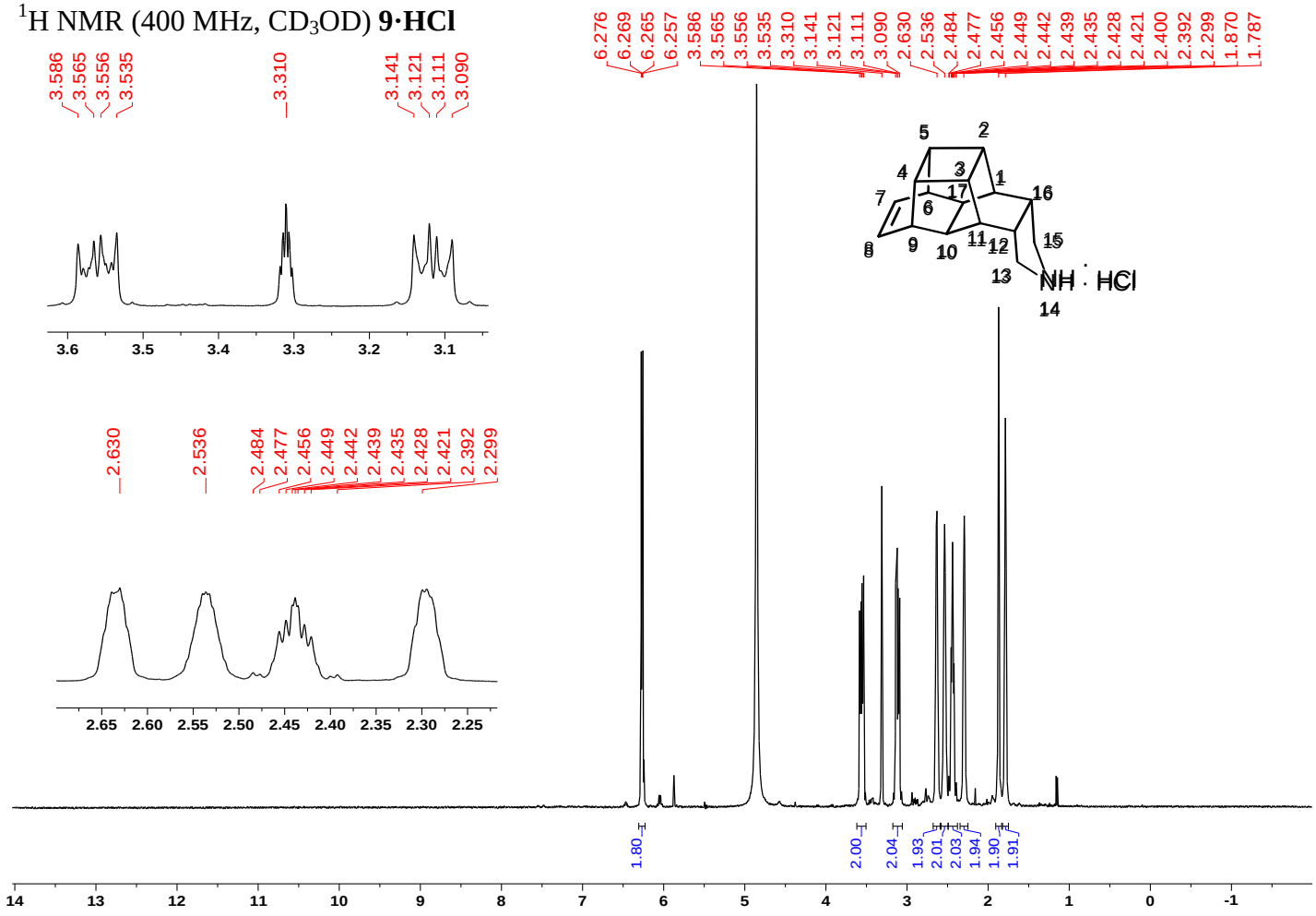

^{13}C NMR (100.6 MHz, CD_3OD) **9·HCl**

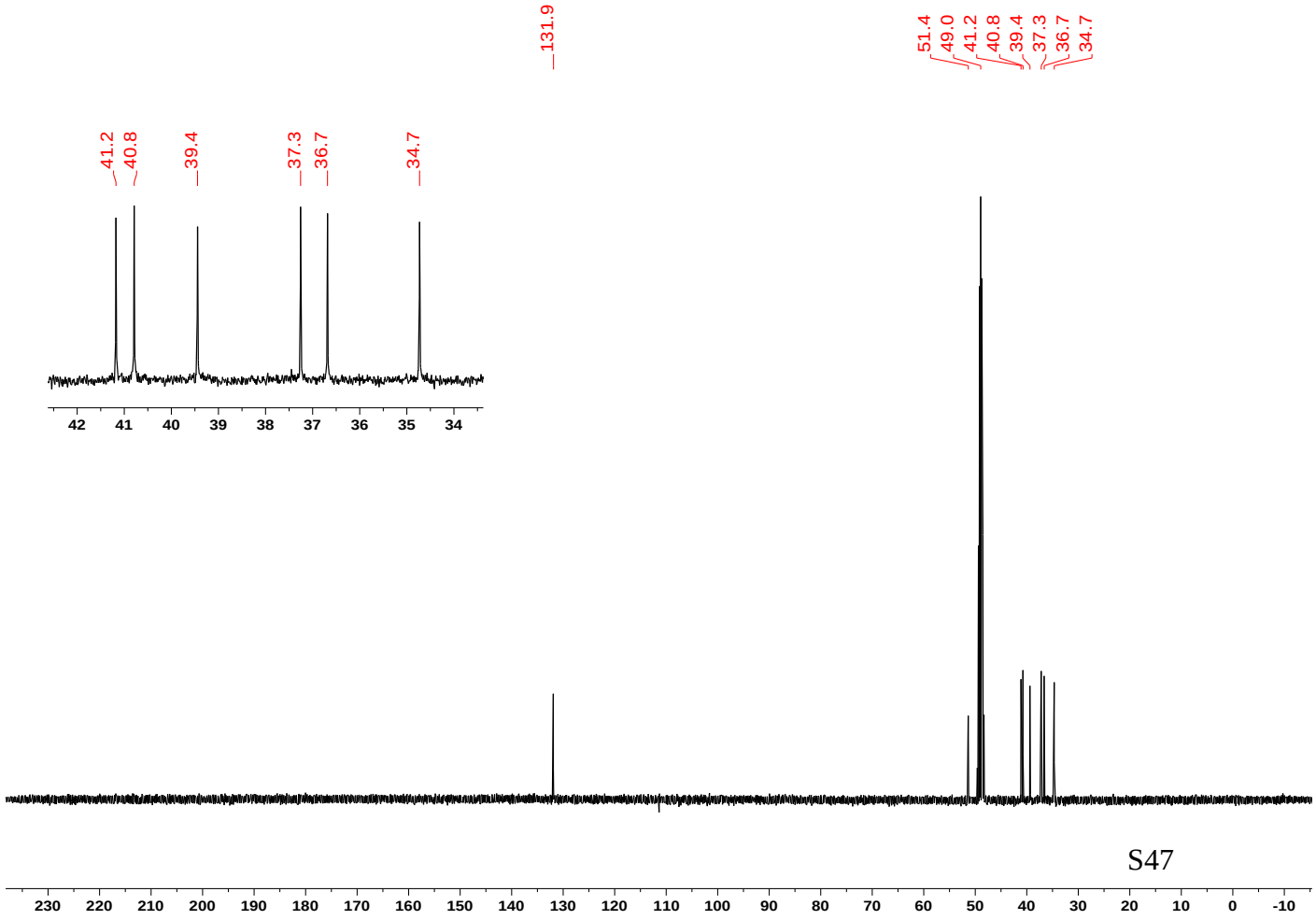

^{1}H NMR (400 MHz, CD_3OD) **10·HCl**

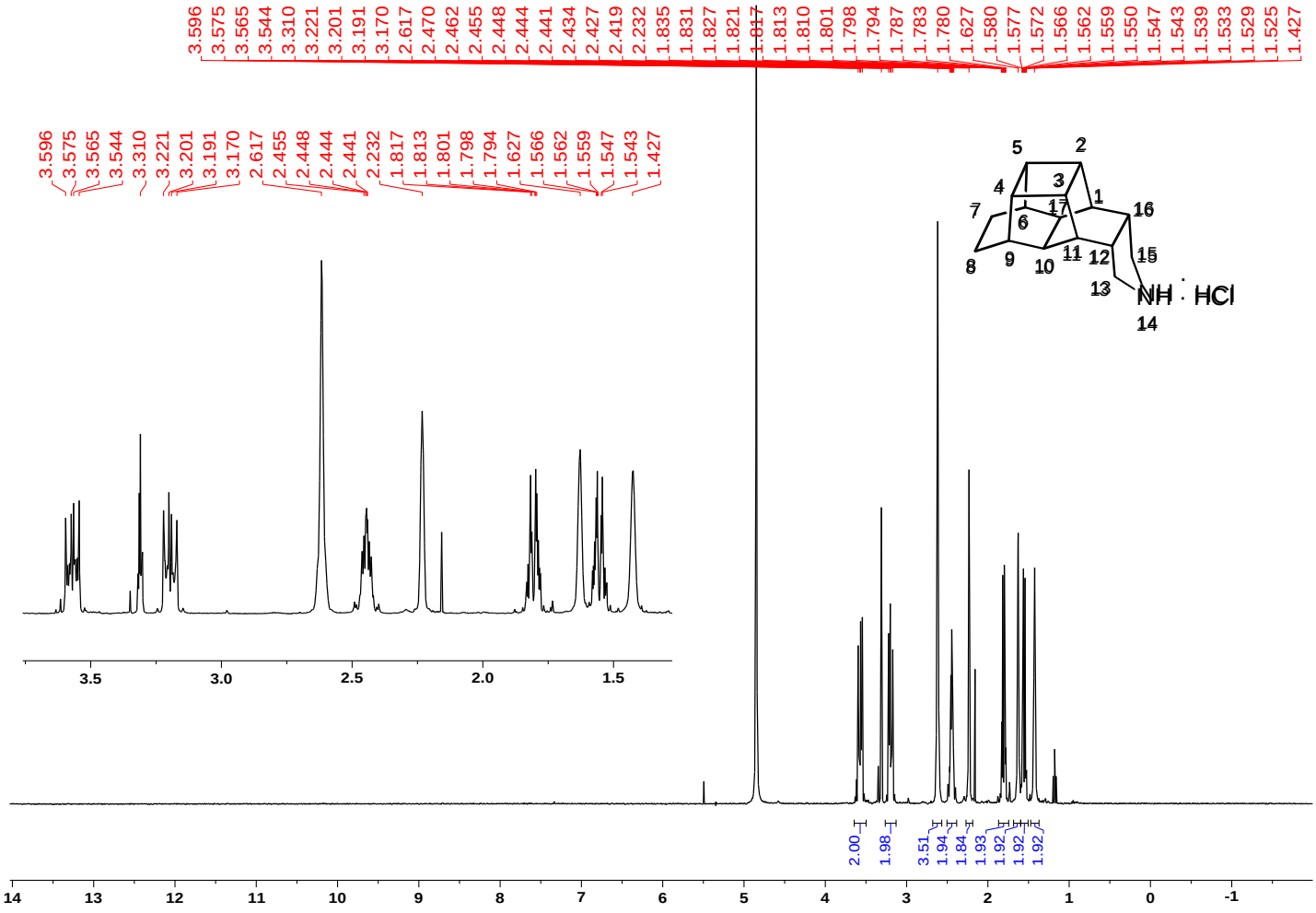

^{13}C NMR (100.6 MHz, CD_3OD) **10·HCl**

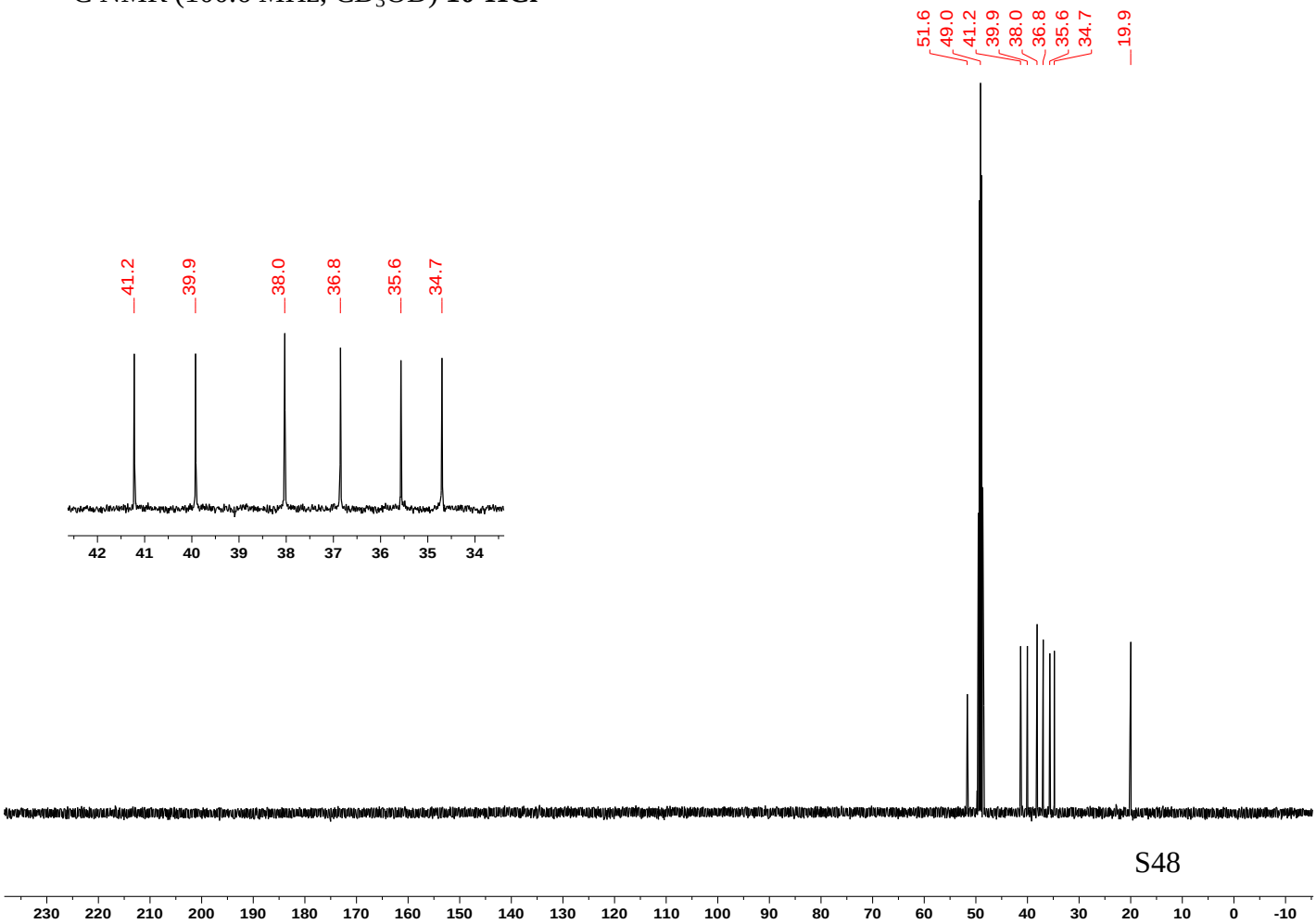

^{1}H NMR (400 MHz, CD_3OD) **11·HCl**

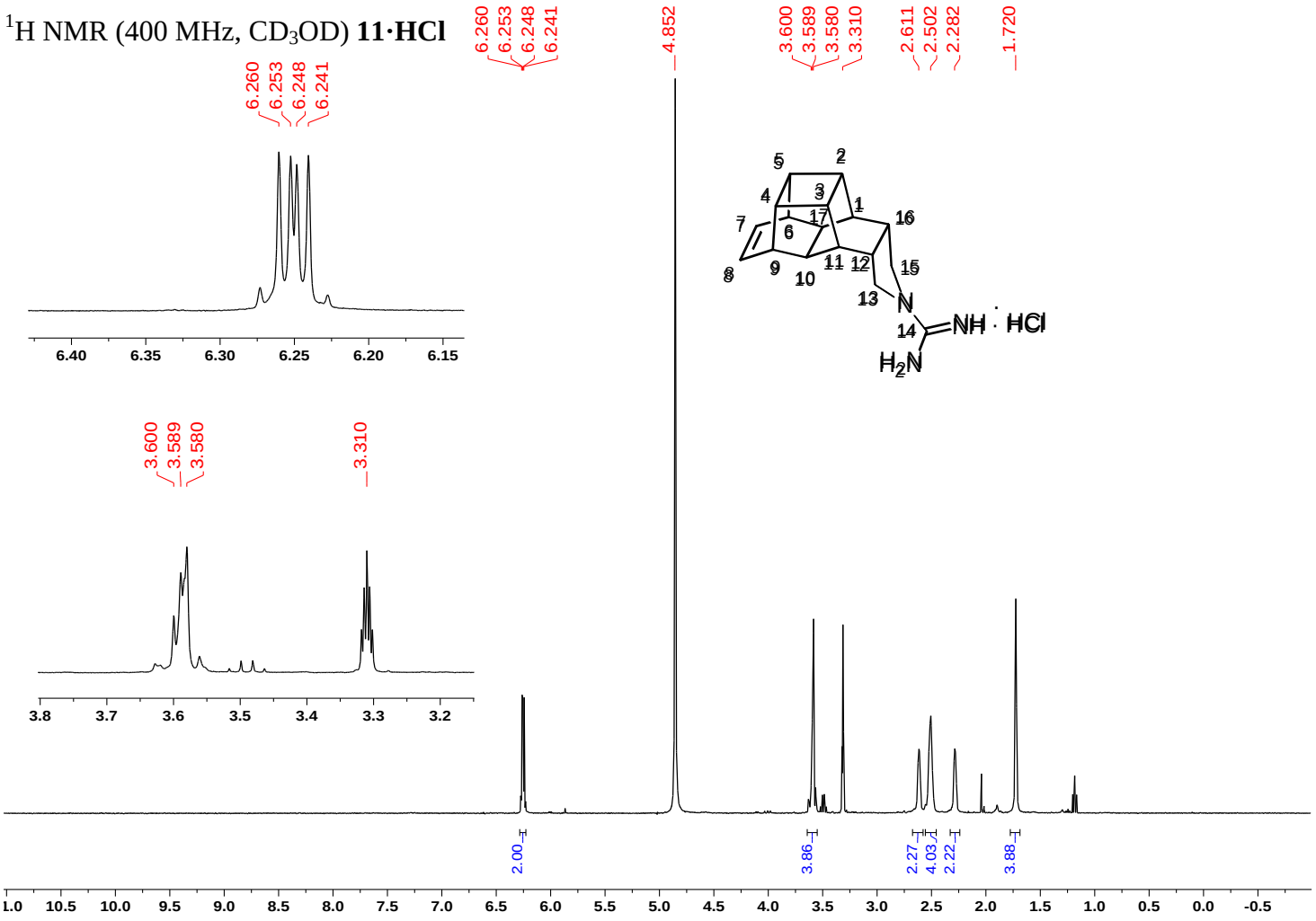

^{13}C NMR (100.6 MHz, CD_3OD) **11·HCl**

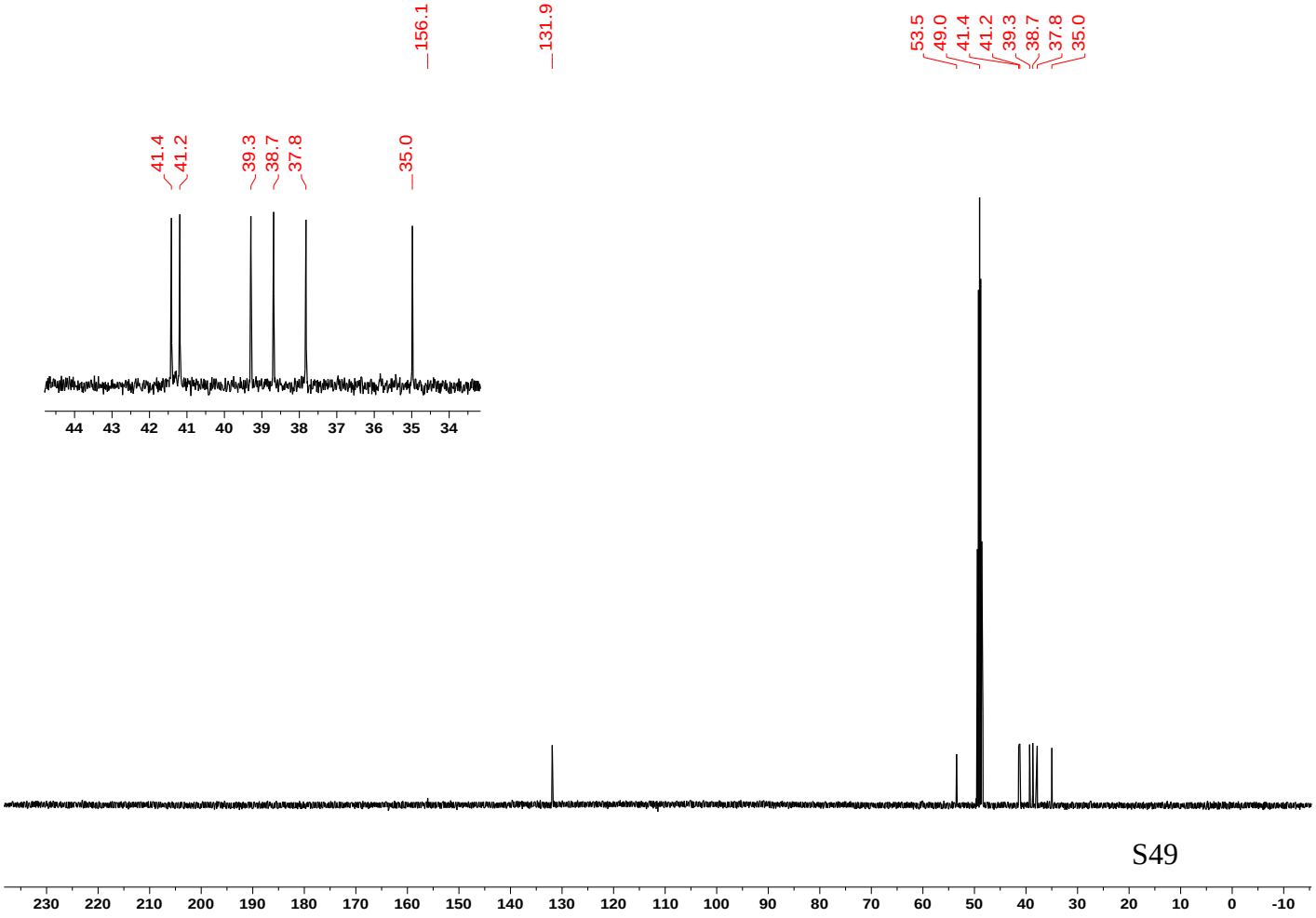

^{1}H NMR (400 MHz, CD_3OD) **12·HCl**

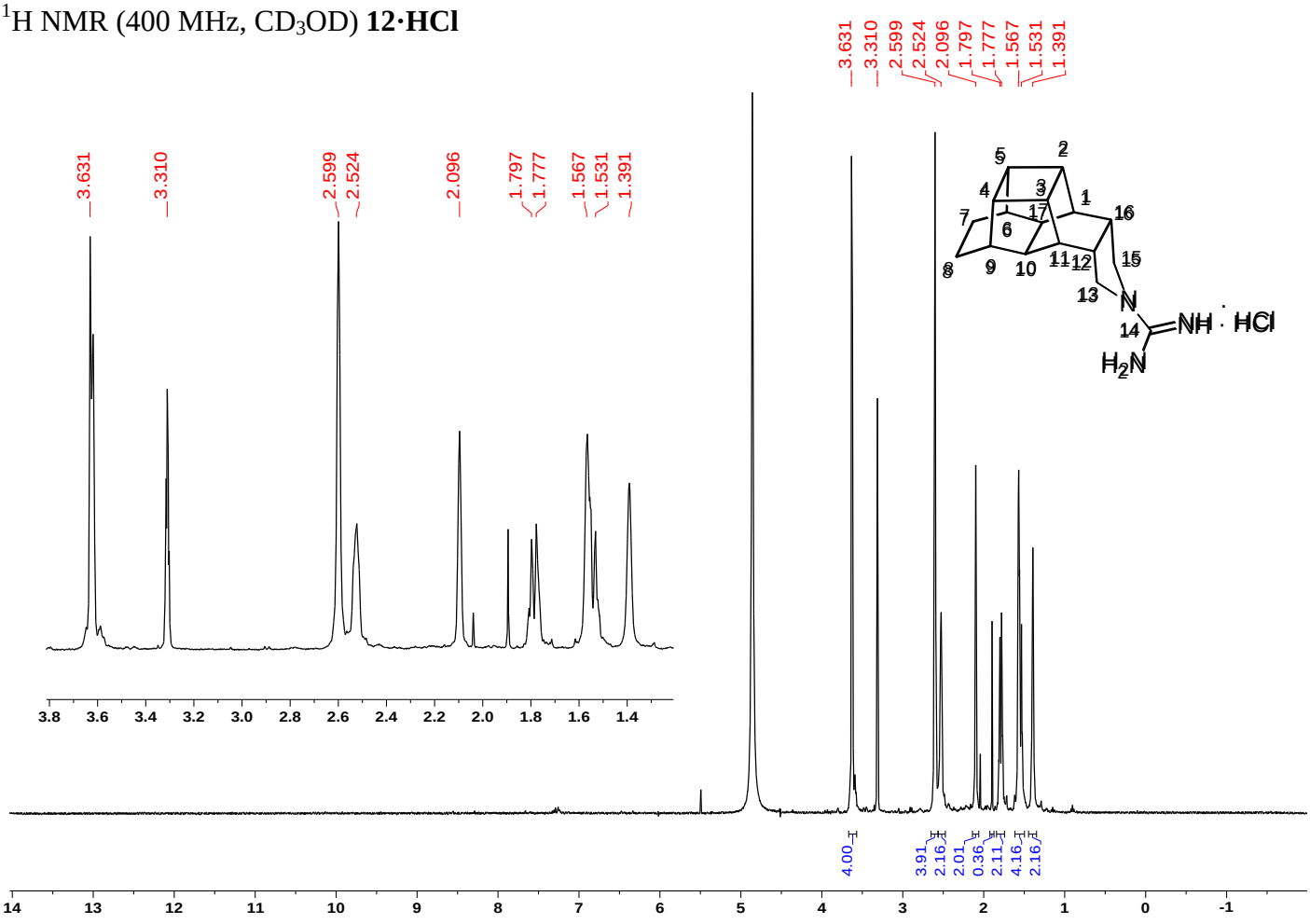

^{13}C NMR (100.6 MHz, CD_3OD) **12·HCl**

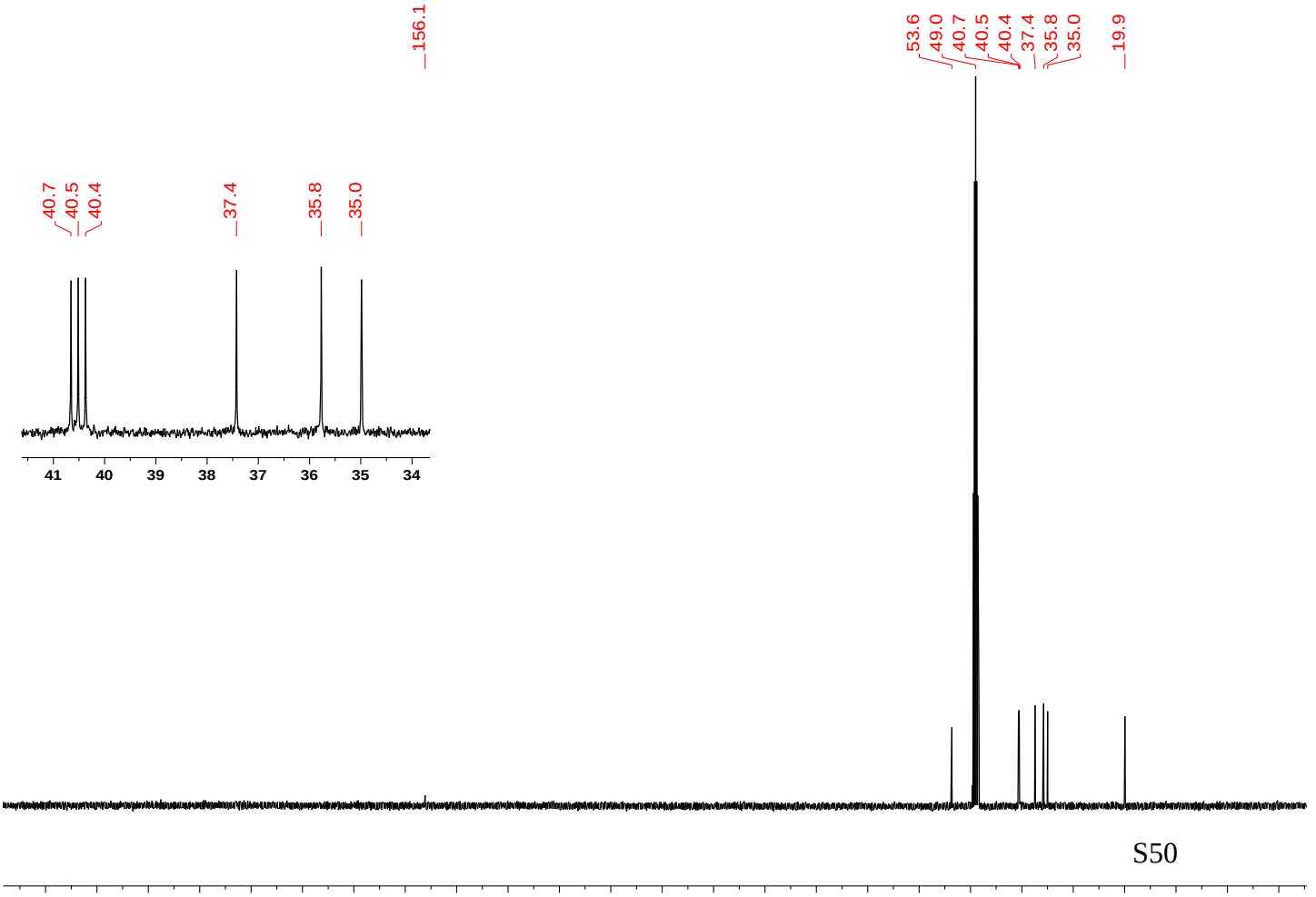

^{1}H NMR (400 MHz, $CDCl_3$) **17**

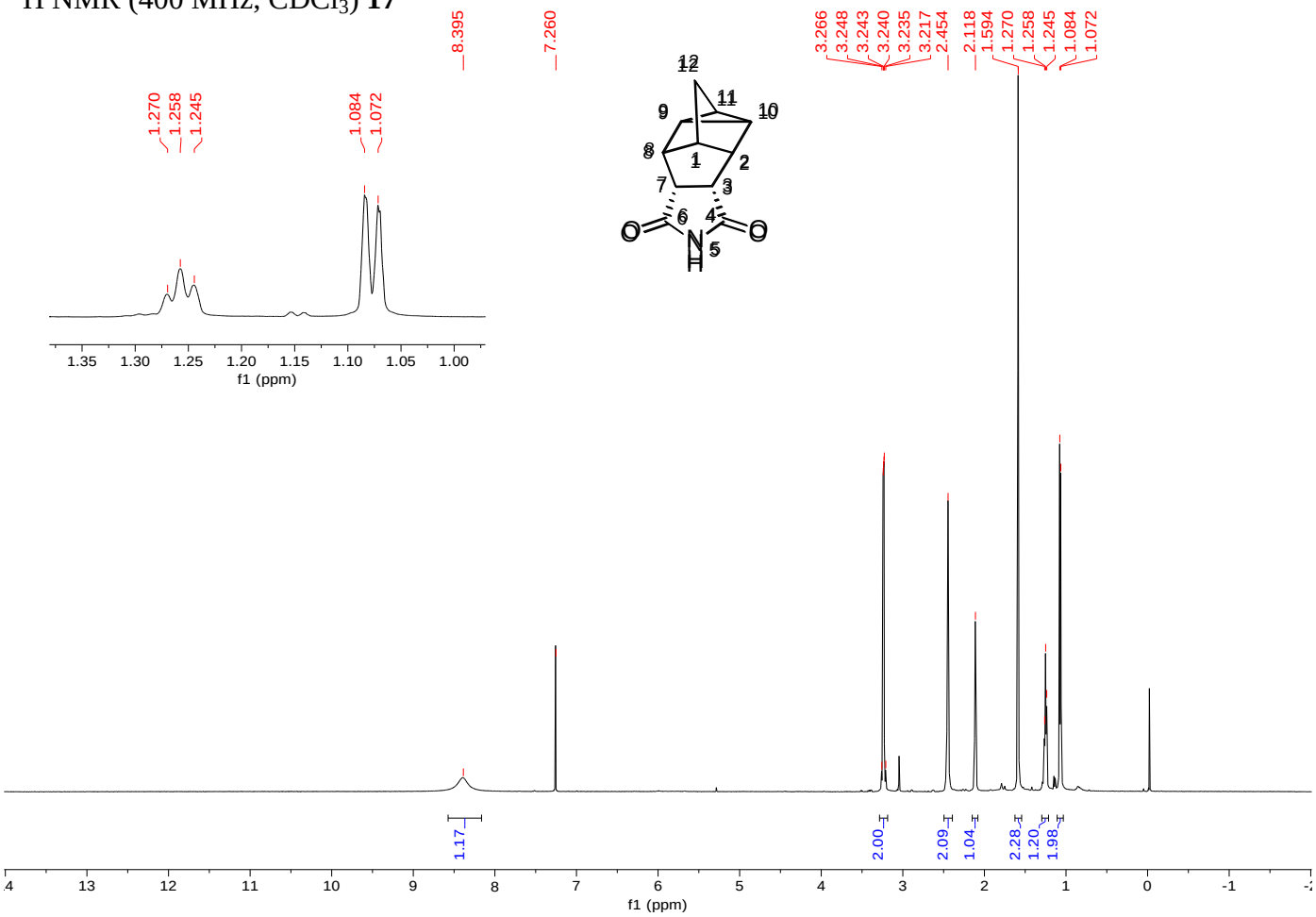

^{13}C NMR (100.6 MHz, $CDCl_3$) **17**

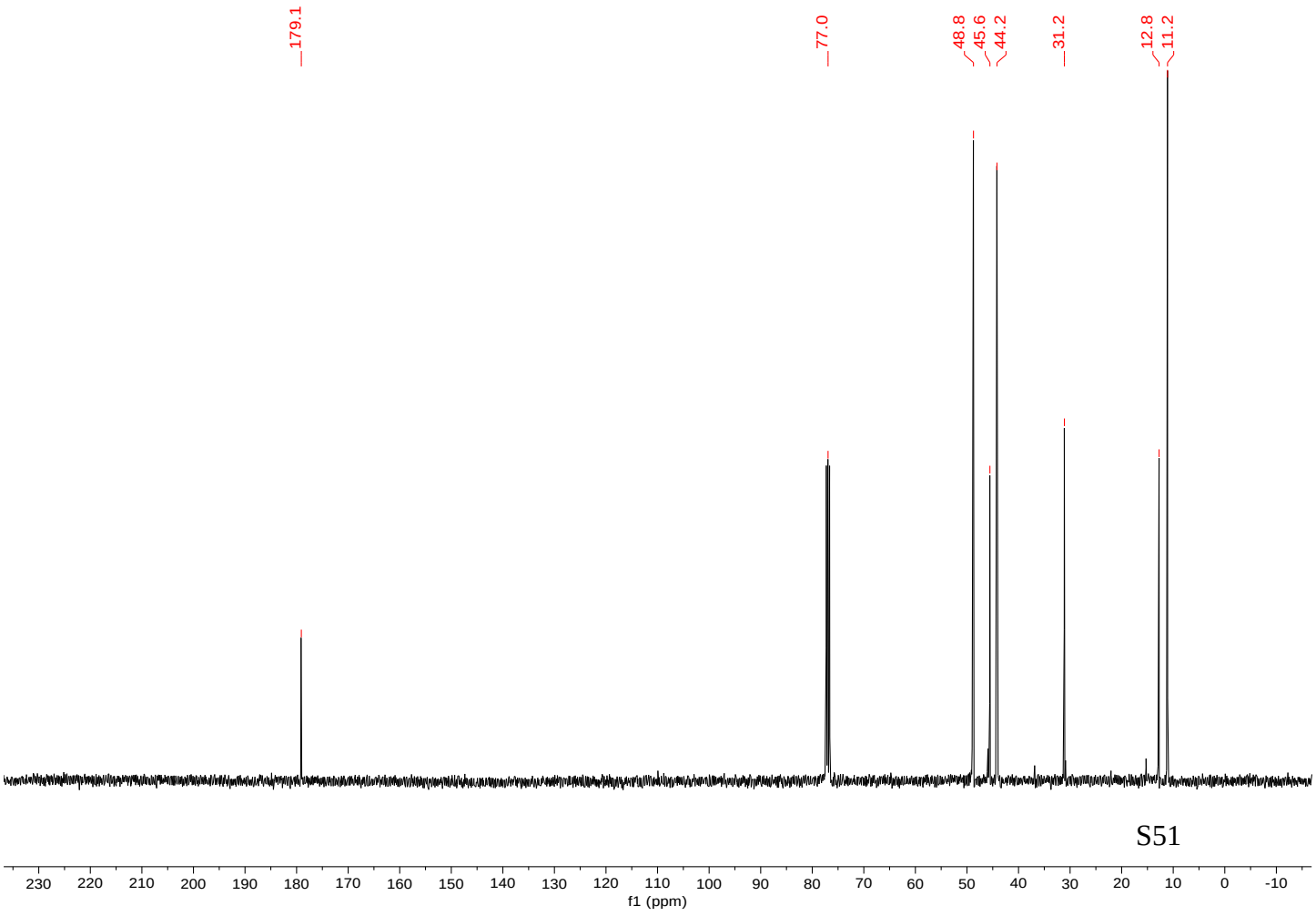

^{1}H NMR (400 MHz, CD_3OD) **18·HCl**

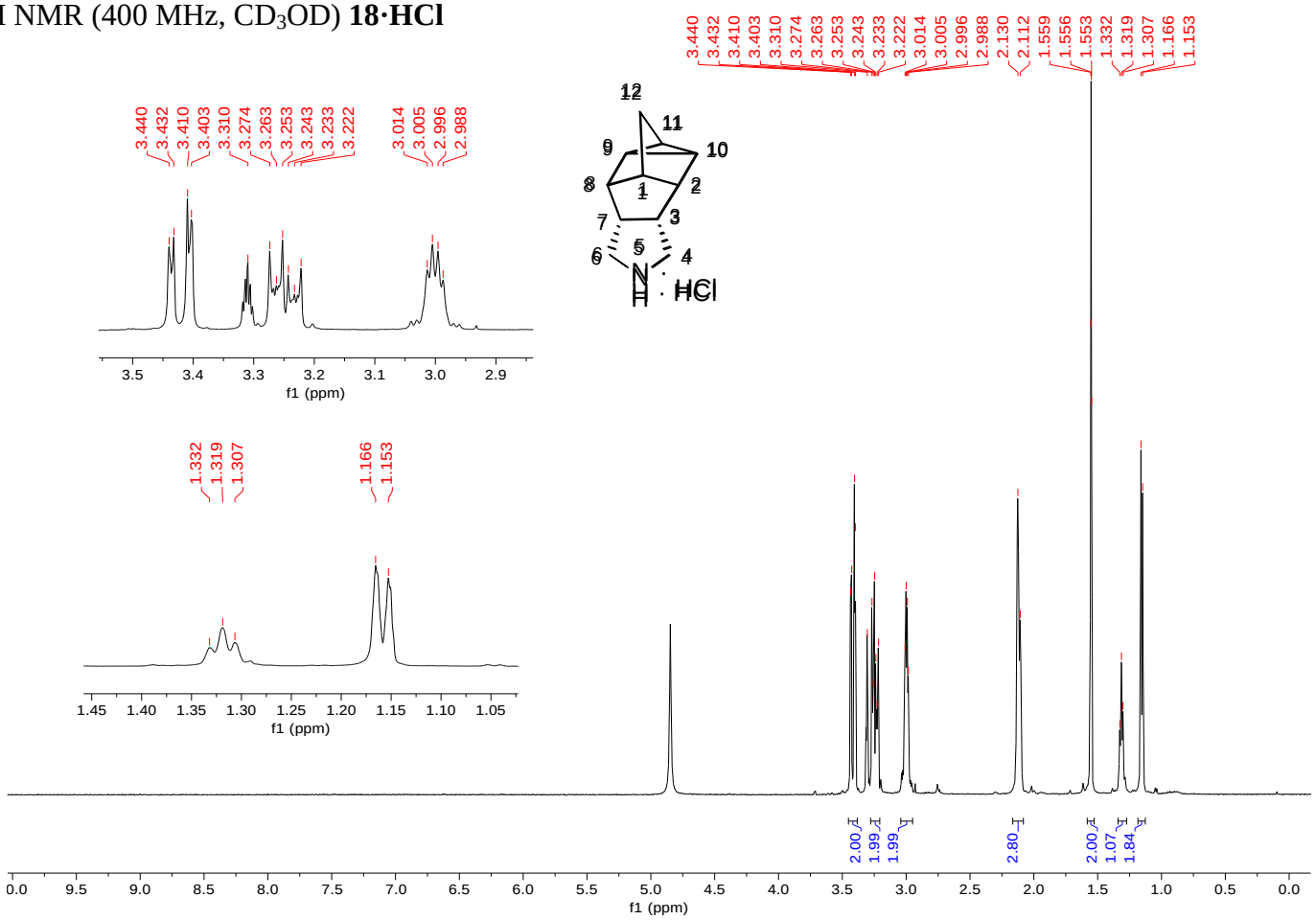

^{13}C NMR (100.6 MHz, CD_3OD) **18·HCl**

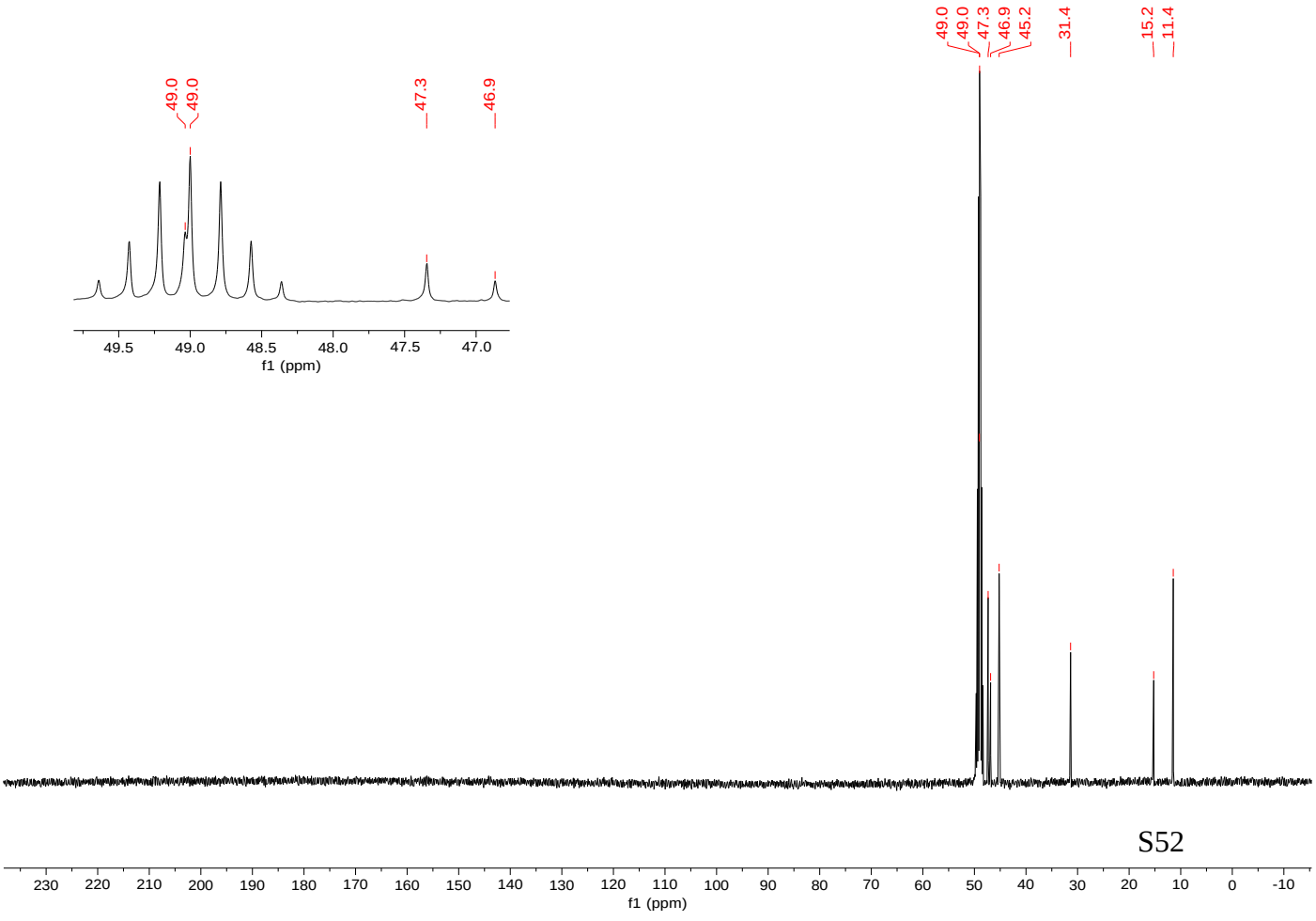

^{1}H NMR (400 MHz, CD_3OD) **19·HCl**

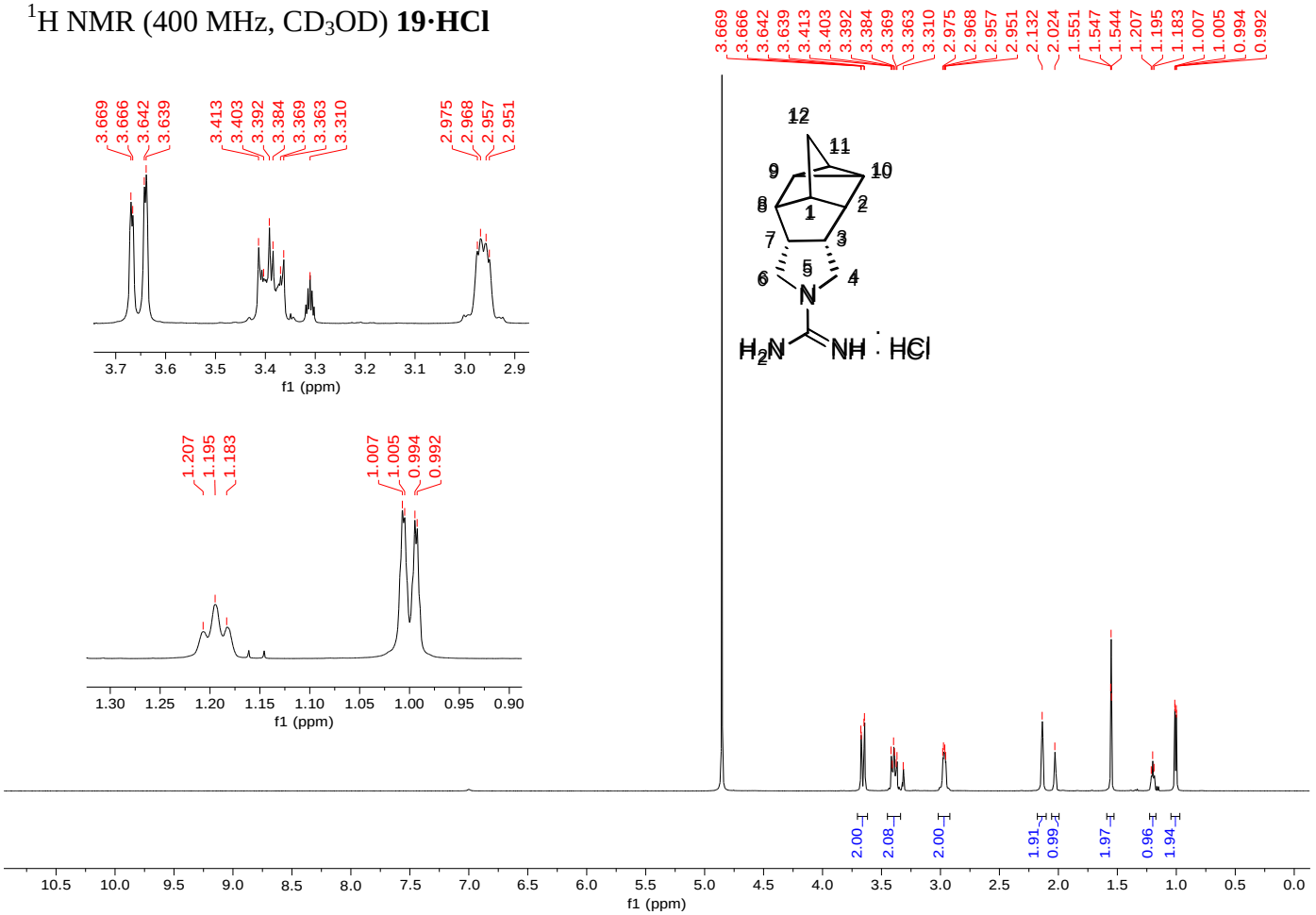

^{13}C NMR (100.6 MHz, CD_3OD) **19·HCl**